MASTER

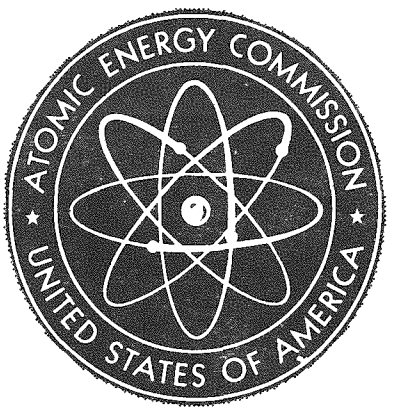

This document is
PUBLICLY RELEASABLE
H. Kinser
Authorizing Official
Date: 6-26-12

HASL-162

NUCLEAR EMULSION SPECTROMETRY AT LOW AND INTERMEDIATE NEUTRON ENERGIES

By
R. Sanna S. Rothenberg
K. O Brien J. McLaughlin
M. Alberg

July 1964

Health and Safety Laboratory
New York Operations Office, AEC
New York, New York

UNITED STATES ATOMIC ENERGY COMMISSION • DIVISION OF TECHNICAL INFORMATION

LEGAL NOTICE

This report was prepared as an account of Government sponsored work. Neither the United States, nor the Commission, nor any person acting on behalf of the Commission:

A. Makes any warranty or representation, expressed or implied, with respect to the accuracy, completeness, or usefulness of the information contained in this report, or that the use of any information, apparatus, method, or process disclosed in this report may not infringe privately owned rights; or

B. Assumes any liabilities with respect to the use of, or for damages resulting from the use of any information, apparatus, method, or process disclosed in this report.

As used in the above, "person acting on behalf of the Commission" includes any employee or contractor of the Commission, or employee of such contractor, to the extent that such employee or contractor of the Commission, or employee of such contractor prepares, disseminates, or provides access to, any information pursuant to his employment or contract with the Commission, or his employment with such contractor.

This report has been reproduced directly from the best available copy.

Printed in USA. Price $4.00. Available from the Clearinghouse for Federal Scientific and Technical Information, National Bureau of Standards, U. S. Department of Commerce, Springfield, Va.

[illegible]

DISCLAIMER

This report was prepared as an account of work sponsored by an agency of the United States Government. Neither the United States Government nor any agency Thereof, nor any of their employees, makes any warranty, express or implied, or assumes any legal liability or responsibility for the accuracy, completeness, or usefulness of any information, apparatus, product, or process disclosed, or represents that its use would not infringe privately owned rights. Reference herein to any specific commercial product, process, or service by trade name, trademark, manufacturer, or otherwise does not necessarily constitute or imply its endorsement, recommendation, or favoring by the United States Government or any agency thereof. The views and opinions of authors expressed herein do not necessarily state or reflect those of the United States Government or any agency thereof.

DISCLAIMER

Portions of this document may be illegible in electronic image products. Images are produced from the best available original document.

HASL-162
HEALTH AND SAFETY
(TID-4500, 44th. Ed.)

NUCLEAR EMULSION SPECTROMETRY AT LOW AND INTERMEDIATE NEUTRON ENERGIES

R. Sanna
K. O'Brien
M. Alberg
S. Rothenberg
J. McLaughlin

July 1964

HEALTH AND SAFETY LABORATORY
U. S. ATOMIC ENERGY COMMISSION
NEW YORK, NEW YORK

... from many coals, one heat comes

Paradiso, Canto XIX

TABLE OF CONTENTS

TEXT

TABLE OF CONTENTS (Cont'd)

TABLES

TABLE OF CONTENTS (Cont'd)

ILLUSTRATIONS

TABLE OF CONTENTS (Cont'd)

INTRODUCTION

For a number of years, the Health and Safety Laboratory of the U. S. Atomic Energy Commission has been concerned with the measurement of stray radiations around particle accelerators[1,2]. Neutrons have been assumed to be the radiation of chief biological interest, and also the most difficult to measure. To obtain measurements of real significance it is necessary to measure, not only the neutron number, but also the neutron energy distribution.

This report describes the use of nuclear emulsions by HASL to measure the neutron energy distribution. A brief historical review of the uses of emulsion is given. This is followed by a description of the physical and chemical properties of nuclear emulsions, and a brief outline of the experimental procedure. The method of processing thick nuclear emulsions using an extended isothermal development is explained, followed by an explanation of the scanning technique used to measure the recoil proton track-length along with a description of the microscope. The analysis of these data to yield a recoil proton spectrum is given.

The relationship between the recoil proton spectrum and the neutron spectrum which is its cause is an integral Fredholm equation; homogeneous, and of the first kind. The kernel of this equation is the differential energy cross-section for the reaction $H^1(n,p)$. We show the relationship of this cross section to the more usual differential angular cross-section in the center-of-mass, and exhibit the formulae of Gammel which we use for computation.

We then replace the integral equation with an explicit summation (essentially the trapezoidal rule) which permits us to rewrite it as a matrix product. We then iteratively solve for the neutron spectrum using Scofield's method. The problem is ill-conditioned, and a method of finding an explicitly smooth solution where this is necessary has been derived.

Finally some results indicating the quality of the method are presented.

USES OF NUCLEAR EMULSIONS

Photographic emulsions were first used to detect radiation by Mugge (1909), who discovered a series of black dots in the emulsions emanating from points where zircon had been sprinkled on the emulsion. He attributed these rows to the activity of the zircon.

Kinoshita (1910) showed that a halide is rendered developable when struck by an alpha particle and Reinganum (1911) discovered that each track produced by an alpha particle is a minute trail of discrete silver grains.

Blau (1925) showed that protons also produced tracks in photographic emulsion and Myssowsky and Tschishow (1927) used emulsions greater than fifty microns in thickness for the first time.

To increase the sensitivity of their emulsions to protons, Blau and Wambacher (1931, 1932) soaked their emulsion in pinakryptol yellow. Ilford Limited and Zhdanov (1935), operating independently, developed a proton sensitive emulsion without using a sensitizing dye. Zhdanov stated that the sensitivity of the emulsion depended on the grain size and concentration of the silver bromide.

Rumbaugh and Locher (1935) covered emulsions with paraffin and exposed them to cosmic rays. They reported finding a considerable number of protons which they attributed to n-p reactions in the paraffin. Richards (1941) used nuclear emulsion to measure neutron spectra from the bombardment of Li^7 with deuterons.

Concentrated emulsions were produced independently by Demers, and Dodd and Waller of Ilford Limited (1945) which improved the track quality and increased the sensitivity of the emulsion as a particle detector.

Dilworth, Occhialini and Payne (1948) deviced the temperature cycle for development of thick emulsions. This enabled experimenters to use emulsions of several hundred

microns in thickness and Yagoda (1958) has used emulsions two thousand micra thick successfully. Rosen (1953), Nerison (1950), Akagi and Lehman (1963) have refined the use of nuclear emulsions as neutron spectrometers, especially as pertains to isotropic sources of neutrons. This report describes the experimental techniques used by the Health and Safety Laboratory to obtain stray neutron spectra around high energy accelerators. It is a combination and extension of the techniques developed by several of the investigators listed above.

PHYSICAL AND CHEMICAL PROPERTIES OF NUCLEAR EMULSIONS

Nuclear emulsion is, like a photographic emulsion, a dispersion of silver halide crystals in a gelatin base. It has, however, two important characteristics, one chemical the other physical, which are quite different from the normal photographic emulsion. Chemically it contains a much higher concentration of silver halide crystals of much smaller average diameter[3]. Physically nuclear emulsion is very much thicker. Table I gives some figures comparing the properties of nuclear and photographic emulsions[4]. A most important parameter for any measurement in nuclear emulsion is its atomic composition. The mean composition of 40 batches of Ilford G-5 emulsion is given in Table II[5].

Ilford Limited, Essex, England manufactures a complete line of nuclear emulsions whose physical and chemical properties are well known, and do not vary to any significant degree from batch to batch[6,7,8,9]. They manufacture three series of emulsions, G, K and L, which have mean grain diameters of 0.27, 0.20 and 0.14 micra, respectively. The range of sensitivities available at present are given in Table III[6]. To date we have used the G-5 and K-2 emulsions in thicknesses of 400 and 600 micra as pellicles and plates. The K-2 emulsion having a smaller grain diameter and being less sensitive does not fog as much as the G-5 in high β-γ field and, therefore, it can often be scanned when the G-5 is overexposed. We have found, however, that a G-5 with a good exposure is easier to scan than a well exposed K-2. We, therefore, only use the K-2 when the G-5 is damaged by excessive background fog. We are at present investigating the use of thicker, 800 to 1,000 micra, emulsions, because their use should reduce the chance of the longer recoil protons escaping through the surfaces. Also under investigation is the use of K-5 and L-4 emulsions in the hope that smaller grain size will reduce the background fog and still give us the high sensitivity of the G-5.

Latent image fading is the rendering of developable grains undevelopable by various physical and chemical processes. Fading of as much as 50% of the tracks in Kodak NTA film had

been reported if the development was delayed for a month or two after exposure. Since our exposures are as long as six months at times, this was thought to be a very serious problem. To investigate the amount of latent image fading in Ilford G-5 emulsions, three sets of emulsions were exposed to Pu-Be neutrons. One emulsion from each set was developed immediately and the other was held for three months before development.

Set #1

As some investigators[10] held that high relative humidity was a major factor in latent image fading, this set was exposed in a sealed plastic container with a dessicant to reduce the humidity to 0%. The emulsion stored for three months had dried out, cracked, and peeled from the glass plate and no determination of the amount of fading was possible. Since then we have ordered all our emulsions with "extra plasticiser" to prevent this cracking and peeling in very dry atmospheres.

Set #2

Other investigators had suggested that the latent image fading might be due more to changes in humidity rather than to just high humidity. This set, therefore, was sealed in a plastic container at the normal relative humidity in our laboratory without dessicant. The emulsion developed three months after exposure did show some fading in the top 10 to 20 microns of emulsion but no fading was detectable below this distance.

Set #3

This set was exposed wrapped only in light tight paper and stored without any protective container. The results were similar to those obtained with Set #2.

Two aspects of our experiment were inconclusive.

1. The effects of high relative humidity 80-90% were not investigated and, therefore, could still be significant.

2. The attempt to study the effect of changes in relative humidity was inconclusive as the unprotected emulsions were stored in an air conditioned building where it was unlikely that the relative humidity would change very much from 50%.

However, since the accelerator buildings in which our exposures are to be made are air conditioned it is felt that the experiment does show that we can in fact expose unprotected emulsions at these sites for periods of three months and even longer without worrying about latent image fading. Although our results were on a qualitative basis they are what would be expected based on results reported by Dahl Jensen[10]. Further experiments are contemplated to determine what environmental conditions can be tolerated without affecting the recoil proton spectra in nuclear emulsion.

Experimental Procedure

An emulsion packet (see Figure 1) consisting of Ilford G-5 and K-2 emulsions and a Dupont type 508 gamma film are sealed in polyethylene and exposed at selected locations near particle accelerators for periods ranging from one week to six months, depending on the radiation intensity at that particular location. After development, the Dupont 508 film is read on a densitometer to obtain a "relative" β-γ exposure. The nuclear emulsions are scanned with a high powered, digitized microscope and approximately 10,000 recoil proton tracks are measured. From these data a recoil proton spectrum is obtained; this in turn will yield a neutron spectrum after mathematical analysis.

EXTENDED ISOTHERMAL PROCESSING OF THICK NUCLEAR EMUSLIONS

The processing of thin nuclear emulsions, up to about 200 micra in thickness, is a relatively simple extension of normal photographic techniques; the difference being in the lenghtening of the time for each step to allow the solutions to diffuse through the emulsion.

Thick emulsions, namely those greater than 200 micra, present a more serious problem, as the diffusion time becomes so long that serious overdevelopment can occur at the surface before the chemicals can reach the interior layers of the emulsion. The solution is fairly obvious: It is necessary to decrease the rate of chemical action of the developer without affecting the diffusion rate to the same extent. Since most developers have a greater negative temperature coefficient of development than diffusion this can be accomplished by cooling the emulsion to about 5°C.

The Health and Safety Laboratory has chosen the Isothermal Development process for the following reasons: 1. Our experience has shown that the temperature control during development at 5°C is much less critical than at 18-20°C and temperature variations of ± 1°C can be tolerated. 2. The necessary equipment for using the method is relatively simple in operation and low in cost. 3. Automation of this process, which is being undertaken in our laboratory, will be much simpler as it is only necessary to hold the temperature at 5°C and not to change it from step to step.

Akagi and Lehman[13,14] have reported this process for 600 micron pellicles. We have used it successfully for 400 and 600 micron pellicles and plates by extrapolating the time for each step, assuming that the diffusion time goes as the square of the thickness. We have also assumed that a 400 micron plate is the equivalent of an 800 micron pellicle and that a 600 micron plate is the equivalent of a 1200 micron pellicle. This assumption is based on the fact that because of the glass

backing developer can diffuse through only one surface of a plate whereas it diffuses through both surfaces of a pellicle. Table IV lists the processing steps and times for 400 and 600 micron pellicles and plates. Table V gives the chemical composition of each solution (all solutions are mixed with distilled water). The purpose of each step in the development process will now be discussed.

1. Presoak

Presoaking the emulsion in distilled water swells it and thereby enables the developer and other solutions to diffuse through it more rapidly.

2. Developer

The developer reduces the silver halide crystals, which have been rendered developable by ionizing radiation, or light in the case of normal photography, to silver grains which will appear as black specks under the microscope.

3. Stop Bath

The stop bath stops the reducing action of the developer and terminates the development, by changing the pH to a point where the accelerator is disabled.

4. Fix

The fixing solution removes all the undeveloped silver halide crystals from the emulsion leaving a transparent gelatin containing the developed silver grains. The silver thiosulphate form is soluble and is washed from the emulsion with water (Step 6).

5. Dilution of the Fix

To avoid undue shock to the emulsion by a too rapid change of the pH of the solutions, thereby causing distortions, the fix solution is diluted in four gradual steps:

a. An equal volume of distilled H_2O is added to the fix solution. This gives a 50% solution of fix.

b. An equal volume of distilled H_2O is added to the 50% fix solution. This gives a 25% solution of fix.

c. Three quarters of the volume of the 25% fix solution is discarded and replaced with distilled H_2O. This gives a 6% solution of fix.

d. The 6% solution of fix is discarded and replaced by distilled H_2O.

6. Wash

The emulsion is washed with frequent changes of deionized H_2O to remove all the fix from it. This is necessary to avoid subsequent fading of the developed silver grains due to the bleaching action of the fix. The wash is continued until a negative permanganate test is obtained.

If a small percentage of hypo is present in the wash water a few drops of the water from the emulsion surface will turn the color of a potassium permanganate solution from its normal violet color to orange in about 30 seconds, if a greater concentration is present this orange color will change to yellow. Therefore, if one thinks the emulsions have washed sufficiently this test can be performed by picking up one of the pellicles or plates and allowing the surface water to drain into 10-20 cc of permanganate solution. We have found that the test is usually successful about 1/2 to 2/3 through the recommended wash cycle (see Table IV).

We feel that it is better to wash for the full time and not use this test too often as any handling of a wet emulsion can cause problems. The only time we use this test is when we are using a thickness of emulsion with which we have little or no experience.

7. Dry

The emulsions are dried by soaking them, in 50% and 75% concentrations of alcohol. This replaces the water in the emulsion with alcohol which will evaporate quite readily in air.

8. Rosin Bath

During the fixing process the undeveloped silver halide crystals are removed from the emulsion. This is by far the greater percentage of the silver halide in the emulsion. If the emulsion is then allowed to dry completely without filling the voids in the gelatin matrix, left by these silver halide crystals, the emulsion will shrink to less than one half of its original thickness. This amount of shrinkage can cause serious errors in the measurement of track lengths, particularly for tracks with a large dip angle i.e. those tracks nearly perpendicular to the surface. A rosin in alcohol solution has proved very successful in filling these voids.

Type N wood rosin which we have obtained from the Hercules Powder Company, Brunswick, Ga., is powdered with a mortar and pestle and then dissolved 30 gms./100 ml in 100% alcohol. This gives a brownish type solution with a white sediment which must be filtered out before the solution can be used. After filtering the solution is a clear amber and may be considered ready for use. The solution must be stored in sealed containers as the evaporation of the alcohol, resulting in precipitation of rosin can be a serious problem.

After the rosin bath the emulsion is allowed to dry at normal room temperature and humidity until dry. Pellicles are placed between taut silk screens to prevent curling during their drying. They are then mounted on glass plates using Eastman 910 cement. This gives a strong optically clear bond without damaging the glued surface of the emulsion. Plates require no special handling after the rosin bath and are just placed on a table to dry. After drying it is necessary to wipe the surfaces of the emulsion and glass plate with a clean soft cloth dampened with 100% alcohol to remove the excess rosin on these surfaces which turns a powdery white on drying. After drying, the identification numbers of each pellicle are etched on the glass plate using a carborundum tipped etching pencil. The plates are now ready for scanning or storage until needed.

Equipment for Isothermal Development

The equipment necessary to develop thick nuclear emulsions under manual technician control is relatively simple and inexpensive when compared with the elaborate systems necessary for the two temperature process.

The developing tank (Figure 2) is a 5 1/2" x 5 1/2" x 7" H stainless steel tank with a drain at the bottom and an intake at the top. A removable lid gives access to the interior and makes a light tight seal when in place. A hole is drilled through this lid so that a thermometer can be inserted into the solutions. Care must be taken to seal the thermometer to the lid with light tight tape to prevent exposure of the film.

Developing racks (Figure 3) - The racks on which the films are placed during development are plastic frames 5" x 4" x 1/4" with an interior hole of 2 3/4" x 3 3/4". Between two of these frames a stainless steel screen is sandwiched. Holes are drilled through the side of the frame to assist the flow of solutions around the emulsion. This rack will accommodate emulsion up to 2" x 3" and when smaller ones are used dividing rods can be inserted so that two or more emulsions can be placed on one rack. As the emulsions are placed on the racks they are stacked and then clamped at the four corners. Each emulsion is, therefore, enclosed in a plastic compartment with 1/2" high sides and screening on top and bottom. The emulsion is free to float around in the developing solutions and at the same time is prevented from coming into contact with other emulsions to which it might stick, damaging both. The clamped stack of developing racks containing the emulsions to be developed is then placed in the developing tank and the light tight lid put on.

Solution Agitator (Figure 4) - It is necessary, particularly during fixing, to continually agitate the solution so that fresh solution is always flowing around the emulsion. This we have accomplished by using a simple rocker consisting of a 10 RPM electric motor with an eccentric cam on which rests a hinged board. As the cam rotates the board is raised and lowered. The developing tank is placed on this board and this up and down rocking motion agitates the solutions.

Solution Storage - Since our developing tank has a capacity of 1.7 liters, we mix two liters of each solution and store them in one liter bottles. The wash water is stored in two 5 gallon bottles and is decanted into one liter bottles as necessary. We also have a 5 gallon drum of 100% alcohol so that the alcohol solutions can be readily prepared as needed. It is most important to remember two things:

1. All solutions must be prepared with distilled water, and

2 The amidol developer must not be mixed until immediately before using.

Temperature Control - The developing tank on its rocker is placed on the bottom shelf of a 12 cubic foot home refrigerator. With the presoak water in the tank the temperature is adjusted so that the water is at 5°C with the rocker working (this is necessary as the electric motor generates a good deal of heat). The solutions are then mixed, except the amidol in the developer, and placed in the refrigerator over night. They will then be at 5°C, if they aren't, some adjustment of the temperature control may be necessary. If one is in a hurry the freezer chest can be used to "fast cool" the solutions.

The amidol should be added to the cooled developer solution immediately prior to use to prevent excessive oxidation.

This is the complete inventory of equipment necessary for the manual development of thick emulsions. We are at present working on an automated system which is more elaborate and costly. This is necessary because the time schedule for developing thick pellicles of 800 or 1000 micra and plates of 600 micra requires personal attendance at odd hours of the day and night. The automated system will be the subject of a future report.

A brief description will now be given of two other methods of developing thick nuclear emulsions. They are known as: 1. the dry hot stage and 2. the wet hot stage, two temperature methods. The main difference is in the temperature and handling of the emulsions during the development stage.

1. Dry hot stage[12]

In this method the emulsions are soaked in the developer at a low temperature for a time sufficient to allow diffusion throughout the emulsion. The emulsion is then removed from the developer and the excess mopped off the surface with a soft cloth. The plates are then warmed to developing temperature (18-20°C) for an appropriate length of time. They are then returned to a cold 5°C stop bath and all ensuing steps are carried out at this temperature. This method requires a great deal of work and many critical steps where an equipment failure or operator error can be disastrous[12].

2. Wet hot stage[12]

A second approach to the two temperature method has been advocated by Barkas. This calls for a wet hot stage. That is the developing temperature is raised while the plate is still immersed in the solution. To avoid over-development at the surface due to replenishment of the developer there, the solution is either diluted or replaced by a weaker one during this step. The succeeding steps are the same as for the dry hot stage. This method has the advantage of avoiding the handling of the emulsion during critical development steps when it is swelled to over twice its normal thickness and is very sensitive to handling of any sort. There is also the advantage that while immersed in a tank of solution at developing temperature, the temperature gradiant within the emulsion will be much less than with a dry hot stage, thereby giving more uniform development. A difficulty is that the temperature control systems must be very precise, since differences of 1°C during the hot stage can be critical. Also during the hot stage the emulsion is greatly swelled and distortions may more readily occur than in the cold emulsion which is structurally more rugged.

SCANNING OF NUCLEAR EMULSIONS

To measure the lengths of the recoil proton tracks it is necessary to use a high powered microscope with very accurate X, Y, and Z coordinate positioning to measure the coordinates of both ends of the tracks. Lawrence Radiation Laboratory has constructed for us a nuclear emulsion microscope with associated electronic equipment for semiautomation. The microscope is a Bausch and Lomb binocular model equipped with a rotating objective turret and specially constructed slide stage, (Figure 5). The optics we have found most useful are a Leitz Ks Fl Oel 100X oil immersion objective with a working distance of 650-micra in combination with Leitz periplan 10x paired oculars with a cross hair in one. This gives a total magnification of 1000 with resolution sufficient to measure tracks of only a few grains.

The microscope stage is the key to this system. Machined out of aluminum with carefully selected lead screws it is accurate over its X and Y traverse to within ± one micron. The Z coordinates are measured using the fine focus control of the microscope which is also accurate to within ± one micron. To the X and Y lead screws and the fine focus control are attached Datex encoders which translate the rotations of the lead screws and fine focus controls into digital information. The system has been very carefully calibrated to read directly in micra.

With the use of associated Datex electronic equipment and an IBM 526 printing summary punch it is possible to punch the three coordinate positions, of the stage (x and y) and fine focus (z), on IBM cards. The system has been programed so that the data is punched with the following format:

columns 1-16	plate identification code
column 17	code # used to indicate last piece of data
columns 18-20	the thickness of the emulsion after development as measured with the fine focus control
column 21	space

columns 22-26	X coordinate
column 27	space
columns 28-32	Y coordinate
column 33	space
columns 34-36	Z coordinate
columns 37,38	space
columns 39-43	X coordinate
column 44	space
columns 45-49	Y coordinate
column 50	space
columns 51-53	Z coordinate
columns 54-80	not used

The technique of measuring the length of a proton recoil track is as follows:

1. Focus the cross hairs of the ocular on one end of the track.

2. Press the record button. This records the coded information (numerical digits 0-9) in columns 1-20. This data is set up on the control box prior to scanning (Figure 6). It then records in columns 22-37 the x, y and z coordinates of that point and stops the card punch.

3. Focus the cross hairs on the other end of the track.

4. Press the record button. This records, in columns 38-53 the x, y and z coordinates of that point, and then ejects the card and injects a new card for the next track.

If an error is made or if it is found that the track escapes the emulsion the reject button on the control panel (Figure 6) ejects the card without punching the second set of coordinates. This enables one to later sort the cards and remove those with only one set of coordinates punched.

We have found it necessary to measure up to 10,000 recoil proton tracks to give us good statistics at the intermediate energies. With a completely manual microscope, one scanner in a two hour shift could record on paper the coordinates of about 60 tracks. Thus it would take, assuming 8 hours per day work load by four scanners, 40 days or eight weeks of tedious, eyestraining work to scan one plate for 10,000 tracks. With the new semi-automatic microscope we have measured as many as 300 tracks an hour with an average of

approximately 125 per hr. Thus the same plate can be scanned in 10 days with this microscope.

The method we use for scanning is quite simple. After one measures a track he then goes to the end point of the track nearest it and repeats his measurement. This method, described as the head to tail method by Akagi and Lehman[13], has been investigated statistically[14] and found to be random except at low energies, less than .5 MeV, where the tracks are so short that nuclear emulsion measurements are impractical. They have used calculated correction factors in this range, while at present we do not. As one scans across the emulsion measuring tracks it is wise to measure, fairly frequently, the developed thickness of the emulsion, which is placed in columns 18-20 on the control box to be punched on the IBM card, so that a shrinkage correction factor can be calculated for the Z component of the tracks. This enables one to catch any local variations from the average developed thickness and makes for more accurate measurements. These variations are usually quite random and we have found them at all times to be less than 10% and averaging about 5%.

THE RECOIL PROTON SPECTRUM

Once having recorded the coordinates of the end points of the track, the recoil proton track length "R" can be found by the Pythagorean theorem:

$$R = \sqrt{(x_1 - x_2)^2 + (y_1 - y_2)^2 + [C(z_1 - z_2)]^2}$$

where

x_1, y_1, z_1 and x_2, y_2, z_2 = the coordinates of the end points of the track and

C = T_1/T_2 is the correction factor for emulsion shrinkage during development

T_1 = the original thickness of the emulsion before development and

T_2 = the thickness after development

The recoil proton energies are then calculated from the proton ranges using equations which fit the experimental data of Lattes, Fowler and Cuer as tabulated by Allred and Armstrong[15] for energies up to 15 MeV. Above 15 MeV the data reported by Barone, et al[16] was used. The four equations used are.

1. $E = 0.0757576\ (\sqrt{26.4^* R + 62.41} - 7.9)$
   for $0.0 \leq R < 14.5\mu$

2. $E = 0.0925926\ (\sqrt{21.6^* R + 109.69} - 9.5)$
   for $14.5 \leq R < 39.7\mu$

3. $E = 0.013089\ (\sqrt{1557.52^* R + 47{,}761.7} - 176.5)$
   for $39.7 \leq R < 1{,}114.6\mu$

4. $E = 0.251R^{0.581}$
   for $1{,}114.6 \leq R$

Equations 1. 2. and 3 are fits of the experimental data of Lattes, Fowler and Cuer using the Gregory-Newton interpolation formula[17]. Equation 4 is that of Bradner, Smith, Barkas and Bishop[18] as reported by Bogaart and Vigniron[19].

Figures 7 through 10 are range energy curves over the range of 0.1 to 197 MeV as taken from Lattes, et al and Baroni, et al. Table VI compares these curves with the calculated values obtained with the above equations.

Once the recoil proton energy has been calculated, it is necessary to correct for the probability that a track of this length will escape through the surface of the emulsion. This is done using the formulae derived by Richards[20].

$$C.F. = \frac{2\ L \sin\theta}{T} \qquad \text{for } L \sin\theta \geq T$$

$$C.F. = \frac{2\ T}{2\ T - L \sin\theta} \qquad \text{for } L \sin\theta \leq T$$

where

C.F. = correction factor
T = original emulsion thickness
L = track length
θ = maximum acceptable dip angle

Table VII lists the correction factors for various energies for both 400 and 600 micra thick emulsions and for a maximum acceptable dip angle of ninety degrees.

The recoil proton energies are then grouped, into suitable energy intervals to form both a corrected, P(E) and uncorrected, P(UE), recoil proton spectrum. Table VIII lists a printout of a typical recoil proton spectrum. Appendix 1 gives the Fortran programs used to obtain the proton spectrum.

Having obtained a recoil proton spectrum it is now necessary to analyze it for the incident neutron spectrum. To better understand our method of analysis it is desirable to first discuss the kinetics of generation of a recoil proton spectrum by the incident neutrons.

Kinetics of N-P Scattering

The recoil protons are generated by neutron collisions with the hydrogen - bearing components of the nuclear emulsion. Such a collision, in laboratory coordinates, is diagrammed this way:

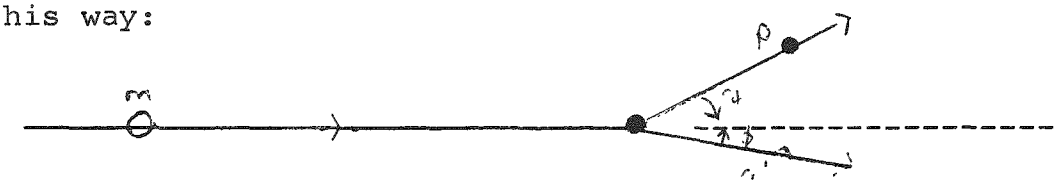

The neutron, in motion, collides with a proton at rest, the proton rebounding at an angle ψ from the original neutron direction. The Newtonian conservation laws can be written in the laboratory system as follows:

$$E_n = E_n' + E_p$$
$$P_n = P_n' \cos\Phi + P_p \cos\psi$$
$$0 = P_p \sin\psi - P_n' \sin\Phi$$

In these equations, E_n is the neutron kinetic energy, and P_n is the neutron momentum before collision; E_n' is the neutron kinetic energy and P_n' is the neutron momentum after collision; and E_p is the proton kinetic energy and P_p is the proton momentum; all in laboratory coordinates. The angles ψ and Φ are the proton and neutron recoil angles in the laboratory coordinate system.

Eliminating Φ, and solving for E_p and E_n, we obtain

$$E_p = E_n \cos^2\psi \qquad (1)$$

The frequency of these collisions for a given angle depends on the cross section $\sigma_n(E_n; \theta)$, after the notation of H. Goldstein[21]. Here, θ is the neutron scattering angle in the center-of-mass system, related to ψ by

$$\theta = \pi - 2\psi \qquad (2)$$

THE TOTAL N-P CROSS SECTION

Gammel[22] has derived a semi-empirical formula for $\sigma_n(E)$, $E<50$ MeV, of great accuracy. It reproduces experimental values up to 42 MeV within the estimated uncertainty attached to these values. Even at 100 MeV, it is in error by less than 20%. The S-wave contribution to $\sigma_n(E)$ was computed using a modified effective-range expansion. The contribution to $\sigma_n(E)$ of states for $L\geq 1$ was estimated and found to be small. The relative contributions from S-wave and higher angular momentum states was computed by Gammel to be:

E-MeV	S-Wave Contribution (barns)	Contribution from States $L\geq 1$ (barns)
14.1	.6795	.006
19.66	.4794	.012
42	.1833	.020

It would seem therefore, that the effective-range formula, if its parameters were a little altered, might fit the curve for the total cross section over this range. The fit was made, and found to be remarkably close.

A brief outline of Gammel's procedure is as follows. Let the S-wave cross sections be written as $\sigma_n(^3S_1)$ and $\sigma_n(^1S_0)$ for the triplet and singlet states respectively, or in general $\sigma_n(S)$. Similarly, $\delta(S)$ will represent the phase shift associated with a given S-state. The wave number k is related to the neutron energy in MeV by

$$k^2 = 1.206\ E \times 10^{24}\ \text{cm}^{-2}. \qquad (3)$$

It can be shown that[23]

$$\sigma_n(S) = \frac{4\pi}{k^2}\sin^2\delta(S) = \frac{4\pi}{k^2 + [k\cot\delta(S)]^2} \qquad (4)$$

In the modified effective range expansion,

$$k \cot \delta(S) = -1/a + 1/2\, \rho k^2 - P\rho^3 k^4 / \left[1 - \left(\frac{2}{\pi} kr_c\right)^2\right] \qquad (5)$$

where a is the scattering length, ρ is the effective range, P is the shape dependent parameter (whenever these variables are superscripted with a 1 or a 3 they represent the values appropriate to the singlet or triplet states), and r_c is the radius of the hard core potential assumed by Gammel. The total contribution to $\sigma_n(E)$ by S-wave scattering is then[24]

$$\sigma_n({}^1S_o + {}^3S_1) = \frac{3}{4}\sigma_n({}^3S_1) + \frac{1}{4}\sigma({}^1S_o)$$

$$= \frac{3\pi}{k^2 + [k \cot \delta({}^3S_1)]^2} + \frac{\pi}{k^2 + [k \cot \delta({}^1S_o)]^2} \qquad (6)$$

If the parameters of equation (5) are altered so that equation (6) fits the experimental values for $\sigma_n(E)$ instead of $\sigma_n({}^1S_o + {}^3S_1)$, from which, as we have seen, it differs only by a little, we have[25]

$${}^3a = 5.376\times10^{-13}\text{cm} \qquad {}^1a = -23.68\times10^{-13}$$
$${}^3\rho = 1.56\times10^{-13}\text{cm} \qquad {}^1P = 2.156\times10^{-13}$$
$${}^3P = -.03 \qquad {}^1P = 0$$
$$r_c = .9457\times10^{-13}\text{cm},$$

and equation (6) becomes

$$\sigma_n(E) = \frac{3\pi}{1.206E + (-1.86 + .09415E + .0001306E^2)^2}$$

$$+ \frac{\pi}{1.206E + (0.4223 + 0.13E)^2} \qquad (7)$$

With the possible exception of the shape dependent parameters ^1P and ^3P, the values inserted in equation (7) differ only a little from the correct values[26]. Table IX shows the agreement between equation (7) and the experimental data. Table IX is Gammel's Table II[27].

THE DIFFERENTIAL N-P CROSS SECTION

Measurements of the differential scattering cross section indicate that isotropy exists for scattering in the center-of-mass system for neutrons having kinetic energies less than 10 MeV in the laboratory system; that symmetry exists about 90° in the center-of-mass for intermediate energies[28] ($10<E<30$ MeV), and small departures from symmetry are expected for higher energy neutrons (~100 MeV). Gammel[29] has fit the n-p differential scattering cross section with a formula symmetric about 90° and consistent with these findings:

$$\sigma_n(E_n;\ \theta) = \frac{\sigma_n\ (E_n)}{4\pi}\ \frac{(1 + b\ \cos^2\theta)}{(1 + \frac{1}{3}\ b)},\ b = 2(E_n/90)^2. \qquad (8)$$

At low energies $b = \sim 0$, and $\sigma_n(E_n;\ \theta)$ is isotropic. In Figure 11 we compare equation (8) with some of the available experimental data[28,30,31,32]. Even at 90 MeV, Gammel's differential cross section appears adequately to describe the data. Table X (Gammel's Table IX[33]) compares the ratio $\sigma_n(E;\ 180^{\circ})/\sigma_n(E;\ 90^{\circ})$ for E up to 90 MeV with the same ratio obtained from rearranging equation (8):

$$\frac{\sigma_n\ (E;\ 180^{\circ})}{\sigma_n\ (E;\ 90^{\circ})} = 1 + 2(E/90)^2, \qquad (9)$$

and equation (9) agrees quite closely with experimental results.

THE DIFFERENTIAL ENERGY CROSS SECTION

The distribution in energy of the recoil protons in emulsion produced by fast neutron bombardment can be obtained from equation (8) which is expressed in terms of the neutron scattering angle in the center of mass. It will be more convenient for our purposes to express it in terms of the recoil proton angle in the laboratory system. This relationship is

$$\sigma_n(E_n; \psi) = 4\sigma_n(E_n; \theta) \cos\psi. \tag{10}$$

If we combine equations (2), (8) and (10), we arrive at

$$\sigma_n(E_n;\psi) = \left[\frac{\sigma_n(E_n)}{\pi} \cos\psi\right]\left[\frac{1 + b \cos^2 2\psi}{1 + \frac{1}{3} b}\right]. \tag{11}$$

Of course, at energies below about 10 MeV, equation 11 becomes

$$\sigma_n(E_n;\psi) = \frac{\sigma_n(E_n) \cos\psi}{\pi} \tag{12}$$

We have drawn attention to equation (12) because it is the usual starting place for the analysis of recoil proton data[34,35,36,37], and because results expressed in its terms have a simplicity that make them valuable for ancillary calculations under conditions where compactness is preferred to precision.

The definitions of the differential scattering cross section, the total scattering cross section, and the differential energy cross section can be written as follows,

$$\sigma_n(E) = \iint_{4\pi} \sigma_{n,p}(E_n;\psi)\, d\Omega = \int_o^{E_n} \sigma_n(E_n; E_p)\, dE_p \tag{13}$$

The element $d\Omega$ is a differential area on a unit sphere in laboratory coordinates constructed about the rest position of the target proton. Similarly, dE_p is an element of energy of the range into which the recoil proton might be lifted. We write

$$d\Omega = \sin\psi\, d\psi\, d\Phi, \tag{14}$$

combine equations (11), (13) and (14), and arrive at

$$2\pi \int_0^{\pi/2} \frac{\sigma_n(E)}{\pi} \left[\frac{1 + b\cos^2 2\psi}{1 + b/3}\right] \cos\psi \sin\psi \, d\psi$$

$$= \int_0^{E_n} \sigma_{n,p}(E_n;\ E_p)\, dE_p \tag{15}$$

From equation (1) we see that the relation between E_p and ψ for a given E_n is bi-unique, and that the limits of the intervals over which the integrations of equation (15) are carried out exactly correspond. We are justified in equating the integrands, giving us

$$2\sigma_n(E) \cos\psi \sin\psi \left[\frac{1 + b\cos^2 2\psi}{1 + b/3}\right] d\psi = \sigma_{n,p}(E_n;\ E_p)\, dE_p . \tag{16}$$

The differential $d\psi/dE_p$ is obtained from equation (1) and is found to be

$$\frac{d\psi}{dE_p} = \frac{1}{2E_n \cos\psi \sin\psi} \tag{17}$$

On combining equations (16) and (17) we have

$$\sigma_{n,p}(E_n;\ E_p) = \frac{\sigma_n(E_n)}{E_n} \left[\frac{1 + b\,(2E_p/E_n - 1)^2}{1 + b/3}\right] U(E_n - E_p). \tag{18}$$

The isotropic approximation (b=0) leads to

$$\sigma_{n,p}(E_n;\ E_p) = \frac{\sigma_n(E_n)}{E_n}\ U(E_n - E_p), \qquad (19)$$

the so called "rectangular" distribution. The function U(X) is the Heaviside unit function, and is defined as

$$U(X) = \begin{cases} 1 & X \geq 0 \\ 0 & X < 0 \end{cases} .$$

The anisotropy factor in the brackets of equation (18) is graphed as a function of neutron and proton energy in Figure 12. It gives a fair indication of the limits of, and the errors to be expected with the use of the isotropic approximation at intermediate and higher neutron energies.

THE INTEGRAL AND MATRIX EQUATIONS

Let the number of hydrogen atoms per cm^3 of emulsion be γ (see Table XI). If the neutron flux is N cm^{-2}, then the recoil proton spectrum cm^{-3} MeV^{-1} in emulsion will be

$$P(E_p) = \gamma \sigma_{n,p}(E_n; E_p)N \qquad (20)$$

Should the neutron flux be distributed in energy and have the units cm^{-2} MeV^{-1}, then the recoil proton distribution is given by the integral Fredholm equation

$$P(E_p) \int_o^\infty \gamma \sigma_{n,p}(E_n; E_p)\, N(E_n)dE_n \,. \qquad (21)$$

At low energies (E_n < 10 MeV), where neutron scattering is isotropic in the center of mass, equation (19) can be used for $\sigma_{n,p}(E_n; E_p)$. Equation (21) then becomes a Volterra equation,

$$P(E_p) = \int_{E_p}^\infty \gamma \frac{\sigma_n(E_n)}{E_n} N(E_n)dE_n, \qquad (22)$$

and can be solved immediately, by differentiating the right and left hand members with respect to E_p, resulting in

$$N(E_p) = - \frac{E_p}{\gamma \sigma_n(E_p)} \frac{d_p(E_p)}{dE_p} \qquad (23)$$

The argument of N refers to the fact that equation (23) gives a numerical value for the neutron flux having the same kinetic energy as the kinetic energy of the differentiated proton spectrum.

$P(E_p)$ is a measured quantity, and is rarely available in a convenient analytical form. Hence values of $N(E)$ must be obtained by a numeric rather than an analytic process.

Let us define

$$\textcircled{H}_{n,p} \equiv \left[1 + b\left(\frac{2E_p}{E_n} - 1\right)^2/(1 + b/3)\right] U(E_n - E_p) \qquad (24)$$

combining equation (18), equation (21) and equation (24), we get

$$P(E_p) = \int_o^\infty \gamma \frac{\sigma_n(E_n)}{E_n} \; N(E_n) \; \textcircled{H}_{n,p} \; dE_n \; , \qquad (25)$$

a Fredholm equation made formally equivalent to a Volterra equation by the inclusion of the Heaviside function in the kernel.

Let

$$x(E_n) = \gamma \frac{\sigma_n(E_n)}{E_n} \; N(E_n)$$

so that equation (25) appears as

$$P(E_p) = \int_o^\infty x(E_n) \; \textcircled{H}_{n,p} \; dE_n \; . \qquad (25a)$$

Next replace the integral in equation (25) with a summation over a constant mesh spacing ΔE_n. Equation (25) then becomes the following matrix product:

$$\begin{bmatrix} P_1 \\ P_2 \\ P_3 \\ \cdot \\ \cdot \\ \cdot \\ P_m \end{bmatrix} = \begin{bmatrix} \textcircled{H}_{11} & \textcircled{H}_{12} & \textcircled{H}_{13} & \cdots & \textcircled{H}_{1m} \\ 0 & \textcircled{H}_{22} & \textcircled{H}_{23} & \cdots & \textcircled{H}_{2m} \\ 0 & 0 & \textcircled{H}_{33} & \cdots & \textcircled{H}_{3m} \\ & & \cdots & & \cdot \\ & & \cdots & & \cdot \\ & & \cdots & & \cdot \\ 0 & 0 & 0 & \cdots & \textcircled{H}_{mm} \end{bmatrix} \begin{bmatrix} x_1 \\ x_2 \\ x_3 \\ \cdot \\ \cdot \\ \cdot \\ x_m \end{bmatrix} \Delta E_n \qquad (26a)$$

or briefly,

$$P = \mathbb{H} X \, \Delta E_n \tag{26b}$$

where the components P_i of the vector P represent the number of recoil protons in the energy interval $(E_i - \Delta E/2, E_i + \Delta E/2)$; the matrix elements of $\mathbb{H}$, $\mathbb{H}_{ij}$, are given by $\mathbb{H}_{n,p}$ (equation 24) when $E_p = E_i$, and $E_n = E_j$; and the components x_j of the vector X are given by:

$$x_j = \gamma \frac{\sigma_j}{E_j} N_j \tag{27a}$$

N_j is the number of neutrons per MeV averaged over the interval $(E_j - \Delta E_n/2, E_j + \Delta E_n/2)$, and σ_j is the n-p scattering cross section calculated at E_j,

$$\sigma_j = \sigma_n(E_j) \ .$$

Hence the neutron spectrum is

$$N_j = \frac{x_j \, E_j}{\gamma \, \sigma_j \, \Delta E_n} \tag{27b}$$

All values of H_{ij} to the left of the diagonal are zero. Physically, this is a consequence of the assumed Newtonian conservations that result in $E_p < E_n$; mathematically this follows from the fact that the incorporation of the Heaviside unit function in the kernel reveals equation (21) to be formally equivalent to a Volterra equation of the first kind[38].

SOLUTION OF THE MATRIX EQUATION

To compute the matrix elements x_j of X we make use of an iterative procedure described by Scofield and Gold[39,40]. Its advantages to us over standard techniques are 2:

1. The values of N_i will always be non-negative, and

2. It requires a very small number of instructions, an important advantage to the user of a small computer.

Let D be a real, diagonal matrix, where the elements are given by

$$d_{ij} = (x_j/p_i)\ \delta_{ij} \tag{28}$$

where δ_{ij} is Kronecker's delta. Then

$$X = D\ P\ . \tag{29}$$

This does not imply (cf equation 26b), of course, that $D = H^{-1}$, because P^{-1} does not exist. The method of Scofield and Gold consists in successive approximations to D. Commence by setting $X^{(0)}$, the zeroth order approximation to X, equal to the recoil proton spectrum P. Let $P^{(0)} = \textcircled{H} X^{(0)}$. Then the elements of $D^{(1)}$ are

$$d_{ij}{}^{(1)} = (x_j{}^{(0)}/p_i{}^{(0)})\ \delta_{ij}\ \ (i,j = 1,\ldots,\ m), \tag{30}$$

and in general[40]

$$\begin{aligned} X^{(\mu)} &= D^{(\mu)}\ P \\ P^{(\mu)} &= \textcircled{H} X^{(\mu)} \\ d_{ij}{}^{(\mu-1)} &= (x_j{}^{(\mu)}/p_i{}^{(\mu)})\ \delta_{ij} \end{aligned} \tag{31}$$

Equation (31) yields the recursion relation,

$$x_\nu(\mu+1) = \frac{x_\nu(\mu)\, p_\nu}{\sum_{j=\nu}^{m} H_{\nu j}\, x_j(\mu)} \qquad (32)$$

the index ν corresponds to the diagonal element for which i=j. The summation in the denominator of equation (32) is thus seen to proceed from the diagonal to the right (all the elements left of the diagonal are zero), and reflects the behavior of the integration in equation (25a). If $|\textcircled{H}| \neq 0$, $\textcircled{H}_{ij} \geq 0$ and x_j, $P_i > 0$, equation (32) converges[40].

Since the matrix H is known analytically, there will be only 2 types of error arising in this use of the Scofield iteration method. One is caused by errors in the observed vector P, and it appears as an error in the vector X toward which the successive approximations $X^{(\mu)}$ converge. The second error is caused by the difference vector $X^{(\mu)}-X$. This latter can be made arbitrarily small by taking μ sufficiently large. Let the true solution vector be X*. Then

$$X^{(\mu)} - X^* = (X - X^*) + (X^{(\mu)} - X) \tag{33}$$

We shall first examine the contributions to the error X - X*, denoted by ΔX. An error ΔV in a function of k variables is given by:

$$\Delta V(z_1, \ldots, z_k) = \sum_{l=1}^{k} \frac{\partial V}{\partial z_l} \cdot \Delta z_l \ , \tag{34}$$

where Δz_l is the error in the variable z_l. Setting $V = x_\nu^{(\mu+1)}$ and substituting equation (32) in (34),

$$\Delta x_\nu^{(\mu+1)} = \frac{p_\nu \, \Delta x_\nu^{(\mu)} + x_\nu^{(\mu)} \cdot \Delta p_\nu}{\sum_{j=\nu}^{m} \widehat{H}_{ij} \, x_j^{(\mu)}}$$

$$- \frac{x_\nu^{(\mu)} \, p_\nu \cdot \sum_{j=\nu}^{m} H_{ij} \, \Delta x_j^{(\mu)}}{\left[\sum_{j=\nu}^{m} \theta_{ij} \, \Delta x_j^{(\mu)}\right]^2} \tag{35}$$

But $\sum_{j=\nu}^{m} H_{ij} \, x_j^{(\mu)} \to p_\nu$, $x_\nu^{(\mu)} \to x_\nu$, and $p_\nu^{(\mu)} \to p_\nu$ as $\mu \to \infty$.

Thus equation (35) becomes

$$\Delta x_\nu^{(\mu+1)} = \Delta x_\nu^{(\mu)} + \frac{x_\nu}{p_\nu} \cdot \Delta p_\nu - \frac{x_\nu}{p_\nu} \sum_{j=\nu}^{m} \textcircled{H}_{ij} \, \Delta x_j^{(\mu)} \qquad (36)$$

Also, as $\mu \to \infty$, $\Delta x_\nu^{(\mu)} \to \Delta x_\nu^{(\mu+1)} \to \Delta x_\nu$, so that

$$\Delta p_\nu = \sum_{j=\nu}^{m} H_{ij} \, \Delta x_j \qquad (37a)$$

or $$\Delta P = \textcircled{H} \cdot \Delta X \qquad (37b)$$

where ΔP and ΔX are the error vectors corresponding to P and X. Solving for ΔX we obtain:

$$\Delta X = \textcircled{H}^{-1} \, \Delta P \, , \qquad (38a)$$

or $$\Delta x_j = \sum_{i=1}^{m} \textcircled{H}_{ji}^{-1} \, \Delta p_i \qquad (38b)$$

where $\textcircled{H}_{ji}^{-1}$ is an element of the inverse matrix $\textcircled{H}^{-1}$.

The standard deviation S_{x_j} is given by[41]:

$$S_{x_j}^2 = \sum_{i=1}^{m} (\textcircled{H}_{ji}^{-1})^2 \, S_{p_i}^2$$

This result is a special case of the error formula derived by Rand[42] for the calculation of spectra by straightforward matrix inversion. Therefore, the restriction imposed by the Scofield method, i.e., that the solution vectors $X^{(\mu)}$ be non-negative, does not introduce additional error in the solution, at least to first order.

We must still consider the convergence error given by $X^{(\mu)} - X$. We know that $P^{(\mu)} = \textcircled{H} X^{(\mu)}$, and that $P = \textcircled{H} X$. Then

$$X^{(\mu)} - X = \textcircled{H}^{-1} (P^{(\mu)} - P) \tag{40a}$$

$$\text{or} \quad x_j^{(\mu)} - x_j = \sum_{i=1}^{m} \textcircled{H}^{-1}_{ji} (p_i^{(\mu)} - p_i). \tag{40b}$$

Comparing equations (40b) and (38b), we see that the convergence error can be neglected if:

$$|p_i^{(\mu)} - p_i| << |\Delta p_i| \tag{41}$$

This criterion can be satisfied by taking a sufficient number μ of iterations. We shall use as our starting point the isotropic approximation, equation (18), for the analysis of error. As a result $\textcircled{H}_{ij} = 1$ to the right of and on the diagonal and $\textcircled{H}_{ij} = 0$ to the left of the diagonal. Then the elements of the inverse matrix $\textcircled{H}^{-1}$,

$$\textcircled{H}^{-1}_{ji} = \begin{cases} 1 \text{ for } i = j \\ -1 \text{ for } i = j+1 \\ 0 \text{ for } i \neq j \text{ or } j+1 \end{cases} \tag{42}$$

Substituting equation (42) in equation (39), we have

$$s^2_{x_\nu} = s^2_{p_\nu} + s^2_{p_{(\nu+1)}} \quad \text{for } \nu = 1, \ldots, (m-1) \tag{43a}$$

$$\text{and} \quad s^2_{x_m} = s^2_{p_m} \tag{43b}$$

and using equations (27b), (34), and (43)

$$S^2_{N_\nu} = \left(\frac{E_\nu}{\Delta E \gamma \sigma_\nu}\right)^2 \left(S^2_{p_\nu} + S^2_{p_{(\nu)}}\right) \quad \text{for } \nu=1, \ldots, (m-1) \qquad (44a)$$

$$\text{and} \quad S^2_{N_m} = \left(\frac{E_m}{\Delta E \gamma \sigma_m}\right)^2 S^2_{p_m} \qquad (44b)$$

The estimation of the standard deviations $S^2_{p_\nu}$ is not a trivial problem, because of the complex factors leading to track production in the emulsion and affecting subsequent observation and measurement of these tracks. We shall assume that these factors combine randomly to give the number q_i of proton tracks counted whose lengths correspond to energies in the interval $\left(E_i - \frac{\Delta E}{2}, E_i + \frac{\Delta E}{2}\right)$ a Poissonian distribution. Then $S^2_q = q_i$, and since $p_i = c_i q_i$, where c is the appropriate correction factor, we have from equation (44):

$$S^2_{N_\nu} = \left(\frac{E_\nu}{\Delta E \gamma \sigma_\nu}\right)^2 \left(c^2_\nu \, q_\nu + c^2_{(\nu+1)} \, q_{(\nu+1)}\right)$$

$$\text{for } \nu=1, \ldots, (m-1) \qquad (45a)$$

$$\text{and} \quad S^2_{N_m} = \left(\frac{E_m \, c_m}{\Delta E \gamma \sigma_m}\right)^2 q_m \qquad (45b)$$

If the isotropic approximation is not used, the expression for S^2_N is far more complex, although it is derived in the same manner.

The coefficient of q_j in equation (45) varies rapidly with energy. As is shown in Figure 13, $Ec/\gamma\sigma_n(E)$ varies as about the fourth power of E, and in the range of our interest is always greater than unity. Consequently small errors in the measurement of q, particularly at high energies, result in large errors in the estimate of N.

Figure 14 shows a set of points computed from equation 32, after 20 iterations, with standard deviations computed from equation (45). To obtain these points, 10,000 tracks were examined. The points are connected by straight broken lines. The violent oscillations in the figure are quite typical results, despite the fact that the neutron spectrum (the stray neutron radiation penetrating the BNL cosmotron wall) is slowly varying with energy. These oscillations correspond to the presence of oscillatory error functions $\xi(E)$ that satisfy

$$\left|\int_{E_p}^{\infty} [\xi(E) + m(E)]\ \gamma\sigma_{n,p}(E;\ E_p)dE\right|$$

$$= c|q' - q| \leq 2S_p \qquad (46)$$

where q represents the true number of proton recoils in the energy interval $[E_p - \Delta E_p/2,\ E_p + \Delta E_p/2]$, q' is the measured number of tracks in that interval, S_p is the standard deviation of the number of recoil protons in that interval, and m(E) is a residual non oscillatory term. For our purposes, a term will be considered oscillatory if it has both positive and negative values in the neighborhood of a measurement point.

These functions are not physically meaningful, and if it were possible to refine the measurement process so that q = q' everywhere, then $\xi(E) = m(E) = 0$ everywhere. The straightforward application of equation (32) always yields solutions of the

form $N'(E) = N(E) + \xi(E) + m(E)$, which by virtue of equation (46) are said to be consistent with σ and q' at the energy E_p where the measurement has been made.

The reduction or removal of $\xi(E)$ in the solution to an integral equation is called smoothing. All the work on this subject of which the authors are aware is concerned with convolution integrals[43,44] relying heavily on the transform properties of such integrals that rely on the Faltung theorem[43,45]. Unfortunately we cannot use their results, mainly because our integrals do not possess well-behaved Fourier transforms and inverses. Instead we have expanded the neutron spectrum, as calculated from equations (32) and (27b), into an orthonormal polynomial series in such a way that the smoothed neutron spectrum is identified with the constant term, and $\xi(E)$ with the higher order terms.

This model was chosen because the higher order terms contain the positive and negative values necessary to represent $\xi(E)$, and the lowest order term, like the neutron spectrum is non-negative.

Consider an orthonormal polynomial set ψ_i over an appropriate energy interval (a, b). Define:

$$y = \frac{E_n - E_p}{\beta} \quad . \tag{47}$$

when the neutron spectrum is expanded about an arbitrary measurement point E_p,

$$N(E_n) + \xi(E_n) + m(E_n) = \sum_i A_i \psi_i (y) \tag{48}$$

where

$$A_i = \int_a^b [N(E_n) + \xi(E_n) + m(E_n)] \psi_i (y) dy \quad .$$

If we choose ψ_i to be the suitably normalized Hermite polynomials, then the interval (a, b) becomes the real line, $(-\infty, \infty)$. The normalized Hermite polynomials are usually

$$\psi_n(x) = H_n(x) \frac{e^{-x^2/2}}{2^{n/2}\ \pi^{1/4}\ (n!)^{1/2}}$$

and the Hermite polynomials, $H_n(x)$ are

$$\begin{aligned} H_0(x) &= 1 \\ H_1(x) &= 2x \\ H_2(x) &= 4x^2-2 \\ &\cdots \\ &\cdots \\ H_{n+1}(x) &= 2x\ H_n(x) - 2n\ H_{n-1}(x). \end{aligned}$$

Let us approximately write,

$$\sigma_{n,p}(E_n;\ E_p) \simeq e^{-(E_n - E_p)^2/2\beta^2}\ \sigma_{n,p}(E_p;\ E_p).$$

Within the limits of validity of this approximation it follows that

$$\int_{-\infty}^{\infty} \gamma\ \sigma_{n,p}(E_n;\ E_p)\ [N(E_n) + \xi(E_n) + m(E_n)]dE_n$$

$$= \int_{-\infty}^{\infty} \beta\gamma\ \sigma_{n,p}(E_p;\ E_p)\pi^{1/4}\ \psi_o(y)\ [\sum_i A_i\ \psi_i\ (y)]dy$$

$$= \beta\gamma\ \sigma_{n,p}(E_p;\ E_p)\pi^{1/4}\ A_o = cq^s(E_p) \qquad (49)$$

After defining $\sigma_{n,p}(E_n;\ E_p) = N(E_n) = \xi(E_n) = m(E_n) = 0$, for $E_n<0$, the lower limit of the integration has been extended to $-\infty$ to be consistent with the definitions of the coefficients

of the orthonormal set. q^s differs from q because of the presence of $m(E_n)$, and because of the cross section replacement in equation (49). Let us define a smoothed neutron spectrum $N^s(E_n)$ corresponding to N, such that

$$N^s(E) = N^T(E) + m(E) = A_o \psi_o(0)$$

$$N^s(E) = \frac{cq^s(E)\ \psi_o(0)}{\beta\gamma\ \sigma_{n,p}(E;\ E)\pi^{1/4}} \qquad (50)$$

$$= \frac{cq^s(E)}{\beta\gamma\ \sigma_{n,p}(E;\ E)\sqrt{\pi}}$$

and $\xi(E) + N(E) - N^T(E) = \sum_{i=1}^{\infty} A_i\ \psi_i(0)$

$N^T(E)$ is a truncation of a series expansion of the neutron spectrum about E. $N^s(E)$ is the usual Gaussian smoothing of the observed neutron spectrum N'(E) as one sees from the definition of A_o:

$$N^s(E) = A_o\ \psi_o(0) = \frac{1}{\beta\sqrt{\pi}} \int_{-\infty}^{\infty} N'(E_n) e^{-(E_n-E)^2/2\beta^2}\ dE_n$$

For the purpose of equation (49), we want $\sigma_{n,p}(E_n;\ E_p)e^{-y^2/2}$ to satisfy the relation:

$$\int_{-\infty}^{\infty} N(E_n)\ \sigma_{n,p}(E_n;\ E_p)dE_n = \int_{-\infty}^{\infty} N(E_n)\sigma_{n,p}(E_p;\ E_p)e^{-(E_n-E_p)^2/2\beta^2}\ dE_n.$$

If $N(E_n)$ is slowly varying, then we can replace this relation with the simpler:

$$\bar{N}\int_{-\infty}^{\infty} \sigma_{n,p}(E_n;\ E_p)dE_n = \bar{N}\int_{-\infty}^{\infty} \sigma_{n,p}(E_p;\ E_p)e^{-(E_n-E_p)^2/2\beta^2}\ dE_n;$$

i.e., equate the lowest order moments, so that

$$\bar{N}\,\mu_\sigma = \bar{N}\,\mu_w .$$

The zeroth moment of the cross section, μ_σ, is,

$$\mu_\sigma = \int_{-\infty}^{\infty} \sigma_{n,p}(E_n;\, E_p)\,dE_n \cong \int_{E_p}^{\infty} \frac{10.97}{E_n(E_n+1.66)}\,dE_n$$

$$\cong \sigma_n(E_p),$$

making the isotropic approximation, and using a simpler relation in place of equation (7)[47]. The zeroth moment of the Gaussian approximation is:

$$\mu_w = \int_{-\infty}^{\infty} \sigma_{n,p}(E_p;\, E_p)\; e^{-(E_n-E_p)^2/2\beta^2}\,dE_n$$

$$= \sqrt{2\pi}\;\beta\;\frac{\sigma_n(E_p)}{E_p}\quad , \tag{52}$$

$$\beta = E_p/\sqrt{2\pi} \tag{53}$$

We get from equation (50),

$$N^s(E) = \frac{\sqrt{2}\;cq^s(E)}{E\,\gamma\,\sigma_{n,p}(E;\, E)} \tag{54}$$

The standard deviation of N^s is:[22]

$$S_N^{2\,s} = \frac{2c^2\,s^2\,q^2(E)}{E^2\,\gamma^2\,\sigma_{n,p}^2(E;\, E)}$$

$$S_N^{2s} = \frac{\sqrt{2}\ cN^s}{\gamma\ \sigma_n(E)} \qquad (55)$$

In equation (55) we have assumed that $\sigma_{n,p}(E;\ E) = \sigma_n(E)/E$, and $S^2_{qs} = q_s$. $S_N{}^s(E)$ is at least to first order equal to $m(E)$. On recapitulating our results, we find

$$N^T(E) \pm S_N{}^s = A_o/\pi\ 1/4$$

$$A_o = \int_{-\infty}^{\infty} N'(E_n)\ \psi_o(y)dy\ , \qquad (56)$$

and $N'(E_n)$ is obtained from equation (32). The approximations in this section affect $S_N{}^s$ and β. They do not affect A_o and N'.

$S_N{}^s$ is smaller than S_N (equation (43)) because it involves weighting a point with all the points in its neighborhood. In Figure 14 we see that application of equation (54) indeed results in a curve without unmanageable oscillations, and is consistent with the data.

Consistency has not been invoked here, and is considered a minimum requirement The key to this section lies in the use of equations (51) and (52) to satisfy an integral condition after limiting $N(E_n)$. There are, obviously, other ways that the condition might be satisfied using different restrictions on $N(E_n)$. Figures 15 and 16 show a measured Pu-Be neutron spectrum as compared with Stewart[48] and a reactor leakage spectrum as compared with Romanko and Dungan[49]. These results do not have high resolution, but seem reliable when the spectrum is in fact smooth.

Figure (17) shows the measured stray neutron spectrum from the Cosmotron, along with its associated standard deviations. It is, essentially, a replotting of Figure 14. Figure 18 shows a stray neutron spectrum measured at the

Princeton-Pennsylvania machine, a comparison spectrum computed by Tsao et al[50] for the same machine, and a comparison spectrum obtained for cosmic ray neutrons at sea-level, by Hess et al[51].

The FORTRAN programs used for these computations are exhibited in Appendix 2. The statements in the neutron spectral programs included between statements number 4 and 90 were taken without alteration from Huddleston et al[46], and serve to terminate the iteration when the distance between the measured proton spectrum and the product $\textcircled{H}X(\mu)$ commences to increase.

CONCLUSION

The representation of Pu-Be and reactor spectra are entirely satisfactory indications that within the limitation of the smoothness requirement, this method of nuclear emulsion spectrometry can be generally relied upon. The accelerator neutron spectra, are quite hard, as we shall expect on theoretical grounds. Where comparison with theoretical expectation is possible, as with the PPA, Figure 18, agreement is good.

ACKNOWLEDGMENT

The authors are particularly grateful to members of the Health Physics Division of the Lawrence Radiation Laboratory at Berkeley for their assistance in providing HASL with a nuclear microscope built and designed at LRL, and for patient advice and criticism at every stage of this project. We want to mention R. Lehman, H. W. Patterson, A. R. Smith, and L. D. Stephens to whom we are especially indebted.

We should also like to take the opportunity of thanking F. P. Cowan, Head of the Brookhaven National Laboratory Health Physics Division, as well as his associates, and M. Awscholom of Princeton's Forrestal Laboratory for their hospitality and assistance.

Special thanks must also be extended to S. Samson of the Statistical Branch of the Health and Safety Laboratory for his invaluable assistance in preparing and compiling the Fortran programs used to analyse our data.

REFERENCES

1. Solon, L. R., McLaughlin, J. E. and Blatz, H. "Stray Radiation Measurements at Particle Accelerator Sites" NYO-4699 (June, 1956).

2. McLaughlin, J. E., O'Brien, K., Solon, L. R., Zila, A. V., Lowder, W. M., and Blatz, H., "Stray Radiation Measurements at Particle Accelerator Sites," NYO-4999, Suppl. 1, (February, 1958).

3. Barkas, W. J., "Nuclear Research Emulsions" Volume I Technique and Theory, Academic Press, New York, London, p. 1 (1963).

4. Doble, N. and Lock, W. O., "1962 Easter School for Physicists Using the Nuclear Emulsion Technique in Conjunction with the CERN Proton Synchrotron and Synchro-Cyclotron," held at St. Cergul, April 8-18, 1962, CERN 63-3, p. 130 (February 6, 1963).

5. Doble, N. and Lock, W. O. op cit p. 130.

6. Ilford Technical Information Sheet Y44-1 (1961).

7. Ilford Research - Supplementary Notes (August 27, 1952).

8. Barkas op cit p. 15.

9. Doble, N., and Lock, W. O. op cit p. 140.

10. Doble, N., and Lock, W. O. op cit p. 137.

11. Dilworth, Occhialini and Vermaesen "Fundamental Mechanisms of Photographic Sensitivity" (J. W. Mitchell, ed.) Academic Press, New York, p. 297-309 (1951).

12. Barkas, W. H. op cit, p.157.

13. Akagi, H., and Lehman, R., "Neutron Dosimetry in and Around Human Phantoms by Use of Nuclear Track Emulsion," Health Physics, Vol. 9, No. 2, p. 207 (February 1963).

14. Lehman, R. private communication.

15. Allred, J. C. and Armstrong, A. H., "Laboratory Handbook of Nuclear Microscopy," LA-1510 (revised edition February, 1953).

16. Baroni, G., Castagnoli, C., Cortini, G., Franzinetti, C. and Manfredini, A., "On the Range Energy Relation for Protons in Nuclear Emulsions," Ricerca Sci, Vol. 26, pp. 1718-31 (1956).

17. Sokolnikoff, I. S. and Redheffer, R. M., "Mathematics of Physics and Modern Engineering," McGraw-Hill, New York, Toronto and London, p. 697 (1958).

18. Bradner, Smith, Barkas and Bishop, AECU-589, UCRL-493, (1949).

19. Bogaart, M. and Vigneron, L., "Le Journal de Physique at le Radium," Vol. 11, p. 652 (1950).

20. Richards, H. T., Phys. Rev. 59, p. 796 (1941).

21. Marion, J. B., and Fowler J. L. eds., "Fast Neutron Physics" Part II Appendix I by Goldstein, H., Interscience Publishers Ltd., London (1960).

22. Marion, J. B. and Fowler, J. L. op cit Chapter VI by Gammel, J. L.

23. Blatt, J. M. and Weiskopf, V. F., Theoretical Nuclear Physics, p. 59, John Wiley and Sons, New York (1951).

24. Blatt, J. M. and Weiskopf, V. F. op cit p. 66.

25. Marion, J. B. and Fowler, J. L. op cit p. 2210.

26. Ibid p. 2185.

27. Ibid p. 2191.

28. Flynn, E. R., Bendt, P. J., Phys. Rev., Vol. 128, p. 1268 (1962).

29. Marion, J. B. and Fowler, J. L. op cit p. 2211.

30. Brolley, Jr., J., Coon, J. H. and Fowler, J. L., Phys. Rev., Vol. 82, p. 190 (1951).

31. Hadly, J., Kelly, E , Leith, C., Segre, E., Wiegand, C. and York, H., Phys. Rev., Vol. 75, p. 351 (1949).

32. Allred, J. C., Armstrong, A. H. and Rosen, L., Phys. Rev., Vol. 91, p. 90 (1953).

33. Marion and Fowler op cit p. 2212.

34. Marion, J. B., and Fowler, J. L. eds., "Fast Neutron Physics," Part I Chapter II D by R. S. White, p. 329 Interscience Publishers Ltd., London (1960).

35. Benjamin, P. W., "Recoil Proton Measurement of Neutron Spectra" in Neutron Dosimetry, Vol. I, International Atomic Energy Agency, Austria (1963).

36. Wallace, R., "Four-Pi Fast Neutron Spectrometers for Detection and Dosimetry" in Neutron Dosimetry, Vol. I, International Atomic Energy Agency, Austria (1963).

37. O'Brien, K., Sanna, R. and McLaughlin, J. E., "The Measurement of Stray Neutrons from a Large Pulsed-Particle Accelerator" in Neutron Dosimetry, Vol. II, International Atomic Energy Agency, Austria (1963).

38. Fox, L., "Numerical Solutions of Ordinary and Partial Differential Equations," p. 165-166, Addison-Wesley Publishing Co. (1962).

39. Scofield, N. E., "Technique for Unfolding Gamma-Ray Scintillation Spectrometer Pulse Height Distributions," USNRDL-TR-447 (June 24, 1960).

40. Gold, R. "Iteration Solution for the Matrix Representation of Detection Systems," TID-18304 (1960).

41. Beers, Y., "Introduction to the Theory of Error", p. 29 Reading, Addison Wesley (1957).

42. Rand, R. E., "The Analysis of Continuous Spectra Using the Matrix Method", N.I.M. 17, p. 65 (1962).

43. Fox, L. op cit p. 164.

44. Kreisel, G., Proc. Roy. Soc. A 197, p. 160 (1948).

45. Morse, P. M. and Feshbach, H., "Methods of Theoretical Physics," Part I, McGraw-Hill, pp. 464, 465 (1961).

46. Huddleston, C. M., Burson, Z. G., Kinkaid, R. M. and Klingler, O. G., "Ground Roughness Effects on the Energy and Angular Distribution of Gamma Radiation from Fallout CEX-62.81 (1964).

47. Simon, A., "Neutron Attenuation," in the Reactor Handbook: Physics", McGraw-Hill, New York, p. 669 (1955).

48. Stewart, L., Phys. Rev., Vol. 98, p. 740 (1955).

49. Romanko, J. and Dungan, W. E., "Specification and Measurement of Reactor Neutron Spectra," in Neutron Dosimetry, Vol. I, p. 156, I.A.E.A., Vienna (1963).

50. Lindenbaum, S. C., "Shielding of High Energy Accelerators" in Annual Review of Nuclear Science, Vol. 11, p. 234 (1961).

51. Hess, W. N., Patterson, H. W., Wallace, R. and Chupp, E. L., "The Cosmic-Ray Neutron Energy Spectrum," UCRL 8628 (1959).

TABLE I

COMPARISON OF PHOTOGRAPHIC AND NUCLEAR EMULSIONS

	Photographic Emulsion	Nuclear Emulsion
Ag Br % by Weight	50	83
Ag Br % by Volume	15	50
Average Crystal Diameter	0.5-3	0.07-0.3
Emulsion Thickness	~10μ	200-1,000μ

TABLE II

CHEMICAL COMPOSITION OF NUCLEAR EMULSIONS

	Normal[5]	Extra Plasticiser[6]
Silver	1.817±.029 g/cc	1.69 g/cc
Bromine	1.338±.020	1.25
Iodine	0.0120±.0002	0.034
Carbon	0.277±.006	0.288
Hydrogen	0.0534±.0012	0.061
Oxygen	0.249±.005	0.30
Nitrogen	0.074±.002	0.061
Sulphur	0.0072±.0002	0.009
Density	3.8278±.0354	

TABLE III

RANGE OF SENSITIVITIES OF ILFORD EMULSIONS

Sensitive to all charged particles of any energy	G5	K5	L4
Less strongly sensitized, recording protons to ~80 MeV (β=0.4). Slow electrons produce tracks of a few grains only		K2	L2
Records protons to ~7 MeV (β=0.12)		K1	
Records protons to ~5 MeV (β=0.1) records thorium α-particles as nearly continuous tracks		K0	

TABLE IV

PROCESSING OF THICK NUCLEAR EMULSIONS

	400μ Pellicle	600μ Pellicle	400μ Plate	600μ Plate
Presoak	20 min.	45 min.	80 min.	3 hrs.
Developer	40 min.	90 min.	160 min.	6 hrs.
Stop	20 min.	45 min.	80 min.	3 hrs.
Fix	10 1/2 hours	24 hrs.	42 hrs.	4 days
Dilution of Fix				
50%	13 min.	30 min.	53 min.	2 hrs.
25%	13 min.	30 min.	53 min.	2 hrs.
6%	20 min.	45 min.	80 min.	3 hrs.
0%	20 min.	45 min.	80 min.	3 hrs.
Wash	40 min.	90 min.	160 min.	6 hrs.
50% Alcohol	13 min.	30 min.	53 min.	2 hrs.
75% Alcohol	27 min.	60 min.	106 min.	4 hrs.
100% Alcohol	27 min.	60 min.	106 min.	4 hrs.
Rosin	10 1/2 hours	24 hrs.	106 hrs.	4 days

TABLE V

COMPOSITION OF DEVELOPING SOLUTIONS

Presoak	Distilled Water
Developer	500 ml distilled water 3.6 gm Na_2SO_3 (anhyd) (Sodium Sulfite Anhydrous) 0.5 gm $Na_2S_2O_5$ ($NaHSO_3$) (Sodium Bisulfite) 4.4 ml* 10% K Br sol'n (Potassium Bromide) 1.6 gm Amidol (akrol)**
Stop Bath	500 ml distilled water 1 ml glacial acetic acid
Fix	500 ml distilled water 150 gms $Na_2S_2O_3$ (thiosulfate) 11.2 gms $Na_2S_2O_5$ ($NaHSO_3$) Sodium Bisulfite
Alcohol	50% Alcohol 75% Alcohol 100% Alcohol
Rosin Solution	100 ml - 100% Alcohol 35 gms - type N wood rosin

* 10 gm K Br, water to make 100 ml = 10% solution.
**Amidol should not be added until immediately prior to use as it oxidizes rapidly.

TABLE VI

RANGE ENERGY RELATIONS, CALCULATED AND EXPERIMENTAL

R	E Calc.	E Act.	% Error	
0	0	0	-	
.8	.94	.1	6%	
1.8	.196	.2	2%	
2.9	.295	.3	1.7%	
4.2	.398	.4	0.5%	
5.6	.50	.5	-	
7.1	.598	.6	0.3%	
8.7	.695	.7	0.7%	$E=0.0757576(\sqrt{26.4*R+62.41} - 7.9)$
10.5	.797	.8	0.4%	
12.5	.902	.9	0.2%	
14.5	1.000	1.0	-	
14.5	1.024	1.0	2.4%	
16.6	1.124	1.1	2.2%	
18.8	1.227	1.2	2.25%	
21.1	1.322	1.3	1.7%	
23.5	1.420	1.4	1.4%	
26.1	1.523	1.5	1.5%	$E=0.0925926(\sqrt{21.6*R+109.6} - 9.5)$
28.7	1.621	1.6	1.3%	
31.3	1.716	1.7	0.9%	
34.1	1.814	1.8	0.8%	
37.0	1.911	1.9	0.6%	
40.0	2.01	2.0	0.5%	

TABLE VI (Cont'd)

RANGE ENERGY RELATIONS, CALCULATED AND EXPERIMENTAL

R	E Calc.	E Act.	% Error
40	2.03	2	1.5%
49.7	2.37	2.3	1.6%
60.0	2.61	2.6	.38%
71.2	2.90	2.9	-
83.6	3.21	3.2	.31%
97.0	3.53	3.5	.86%
120.6	4.04	4.C	1.0%
173.0	5.0	5	1.01%
234.0	6.09	6	1.5%
305.9	7.17	7	2.4%
385.0	8.22	8	2.8%
468.7	9.23	9	2.6%
564.1	10.28	10	2.8%
665.6	11.32	11	2.9%
776.0	12.36	12	3.0%
894.5	13.40	13	3.0%
1,015	14.38	14	2.7%
1,136	15.33	15	2.2%
1,000	13.85	14.2	2.5%
1,500	17.6	17.8	1.1%
2,000	20.75	21.0	1.2%
2,500	23.65	23.8	0.6%
3,000	26.3	26.4	0.4%
3,500	28.8	28.8	-

$E=0.013089(\sqrt{1.557.52R+47,761.7} - 176.5)$

TABLE VI (Cont'd)

RANGE ENERGY RELATIONS, CALCULATED AND EXPERIMENTAL

R	E Calc.	E Act.	% Error	
4,000	31.1	31.2	0.3%	
5,000	35.4	35.3	0.3%	
6,000	39.3	39.3	-	
7,000	43.0	42.8	0.5%	
8,000	46.5	46.2	0.6%	
9,000	49.8	49.3	1.0%	
10,000	52.9	52.5	0.8%	$E=0.251R^{.581}$
15,000	67.0	66.0	1.5%	
20,000	79.1	77.5	2.1%	
25,000	90.1	88.0	2.2%	
30,000	100	98.0	2.0%	
35,000	109	108.3	0.6%	
40,000	118	115.7	2.0%	
50,000	135	131.5	2.7%	
60,000	149	146	2.1%	
70,000	164	160	2.5%	
80,000	177	173	2.3%	
90,000	189	185	2.2%	
100,000	202	197	2.5%	

TABLE VII

CORRECTION FACTORS FOR TRACKS ESCAPING THE EMULSION

E(MeV)	(400 Micra)	(600 Micra)
.5	1.0068	1.0045
1.0	1.0183	1.0121
2.0	1.0526	1.0344
3.0	1.1037	1.0668
4.0	1.1775	1.1117
5.0	1.2743	1.1675
6.0	1.4176	1.2444
7.0	1.6237	1.3442
8.0	1.9356	1.4754
9.0	2.3679	1.6519
10.0	2.8387	1.8979
12.0	3.8849	2.5899
14.0	5.0653	3.3768
16.0	6.3739	4.2493
18.0	7.8062	5.2041
20.0	9.3581	6.2387
25.0	13.7396	9.1597
30.0	18.8037	12.5358
35.0	24.5166	16.3444
40.0	30.8506	20.5671
45.0	37.7831	25.1887
50.0	45.2946	30.1964
55.0	53.3683	35.5788
60.0	61.9894	41.3263
65.0	71.1448	47.4298
70.0	80.8226	53.8817
75.0	91.0122	60.6748
80.0	101.7038	67.8025
85.0	112.8883	76.0224
90.0	124.5577	83.0385
95.0	136.7040	91.1360
100.0	149.3204	99.5469

TABLE VIII

PRINTOUT OF FORTRAN PROGRAM TO OBTAIN THE RECOIL PROTON SPECTRUM

Cambridge Electron Accelerator No. 17
400 Micron Plate

Energy	Corrected Spectrum	Uncorrected Spectrum
E= 1.00	P(E)= 8987.434	P(UE)= 8878.000
E= 3.00	P(E)= 617.049	P(UE)= 566.000
E= 5.00	P(E)= 263.718	P(UE)= 210.000
E= 7.00	P(E)= 164.438	P(UE)= 105.000
E= 9.00	P(E)= 132.475	P(UE)= 60.000
E= 11.00	P(E)= 91.272	P(UE)= 30.000
E= 13.00	P(E)= 80.668	P(UE)= 19.000
E= 15.00	P(E)= 64.827	P(UE)= 12.000
E= 17.00	P(E)= 35.485	P(UE)= 5.000
E= 19.00	P(E)= 60.654	P(UE)= 7.000
E= 21.00	P(E)= 30.538	P(UE)= 3.000
E= 23.00	P(E)= 23.822	P(UE)= 2.000
E= 25.00	P(E)= 12.938	P(UE)= 1.000
E= 27.00	P(E)= 16.164	P(UE)= 1.000
E= 29.00	P(E)= 0.000	P(UE)= 0.000
E= 31.00	P(E)= 60.798	P(UE)= 3.000
E= 33.00	P(E)= 0.000	P(UE)= 0.000
E= 35.00	P(E)= 48.071	P(UE)= 2.000
E= 37.00	P(E)= 27.321	P(UE)= 1.000
E= 39.00	P(E)= 0.000	P(UE)= 0.000
E= 41.00	P(E)= 0.000	P(UE)= 0.000
E= 43.00	P(E)= 36.366	P(UE)= 1.000

TABLE IX

COMPARISON OF EXPERIMENTAL AND CALCULATED VALUES OF $\sigma_n(E)$

E (MeV)	$\sigma_n(E)$ (barns) Calculated (Eq. 7)	$\sigma_n(E)$ (barns) Experimental
Thermal	20.34	20.36 ± 0.10
1.005	4.232	4.228 ± 0.018
1.315 ± 0.003	3.671	3.675 ± 0.020
2.540	2.523	2.525 ± 0.009
4.749 ± 0.009	1.683	1.690 ± 0.006
14.10 ± 0.05	0.688	0.689 ± 0.005
14.12 ± 0.04	0.687	0.686 ± 0.007
19.655± 0.035	0.494	0.495 ± 0.003
25	0.381	0.39 ± 0.03
42	0.202	0.203 ± 0.007

TABLE V

COMPARISON OF EXPERIMENTAL AND CALCULATED VALUES OF $\sigma_n(E; 180^o)/\sigma_n(E; 90^o)$

	$\sigma_n(E; 180^o)/\sigma_n(E; 90^o)$	
E(MeV)	Calculated (Eq. 33)	Experimental
1	1.0002	
4	1.003	
8	1.016	
10	1.025	
14.1	1.049	
		1.06 ± 0.023
		1.04 ± 0.05
		1.06 ± 0.06
17.9	1.079	1.08 ± 0.03
19.66	1.095	1.09 ± 0.03
22	1.119	
27.2	1.183	1.28 ± 0.10
42	1.441	1.55 ± 0.20
91	3.044	3.15 ± 0.10

TABLE XI

HYDROGEN CONCENTRATION OF ILFORD G-5 EMULSION AT 58% RELATIVE HUMIDITY

	Hydrogen atoms/cm^3 x 10^{22}
Normal emulsion	3.346
2 times normal gel concentration	3.706
4 times normal gel concentration	4.303
8 times normal gel concentration	4.781
Normal emulsion with extra plasticiser	3.645

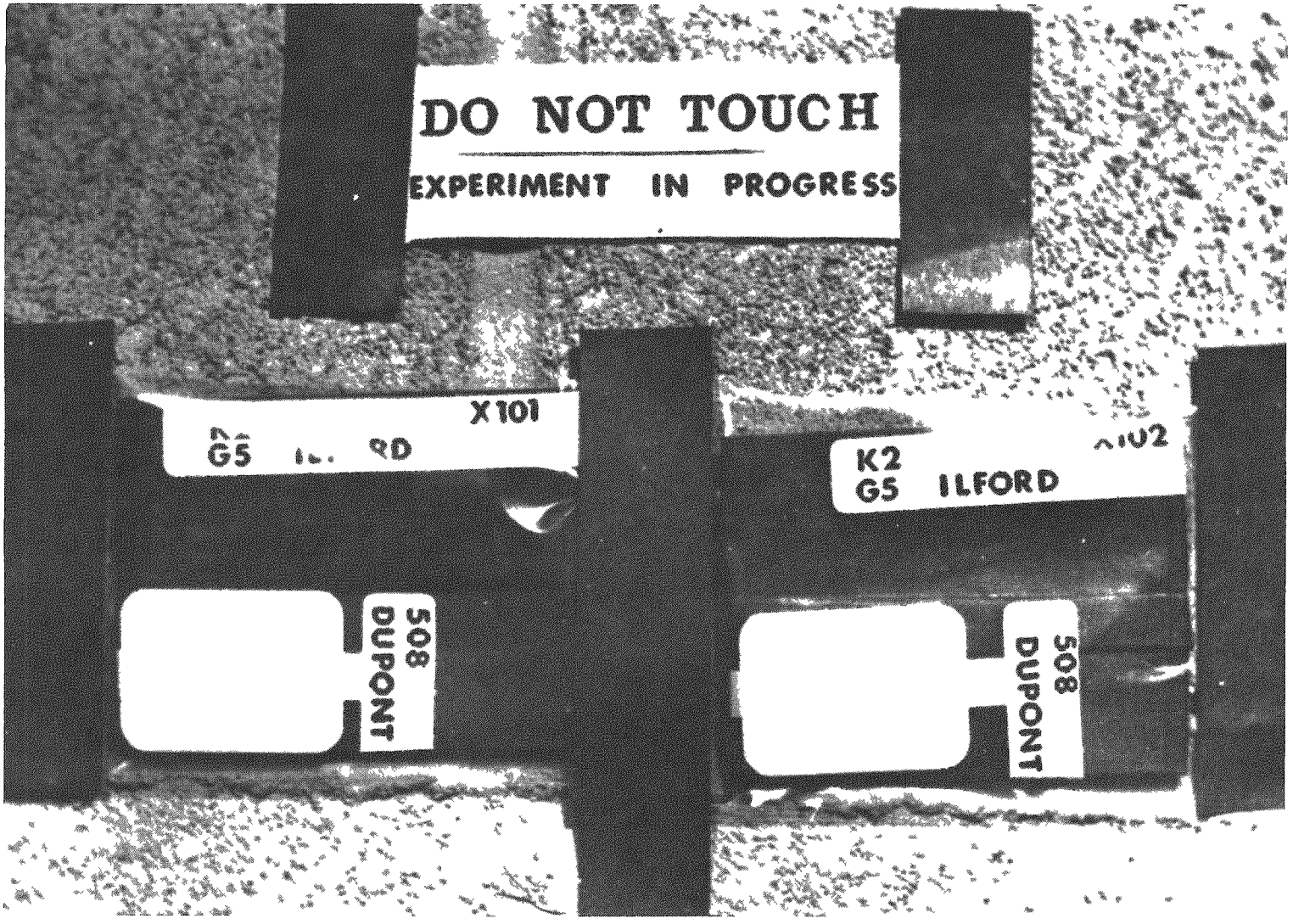

Fig. 1 NUCLEAR EMULSIONS TAPED TO WALL IN OFFICE (AT ACCELERATOR SITES)

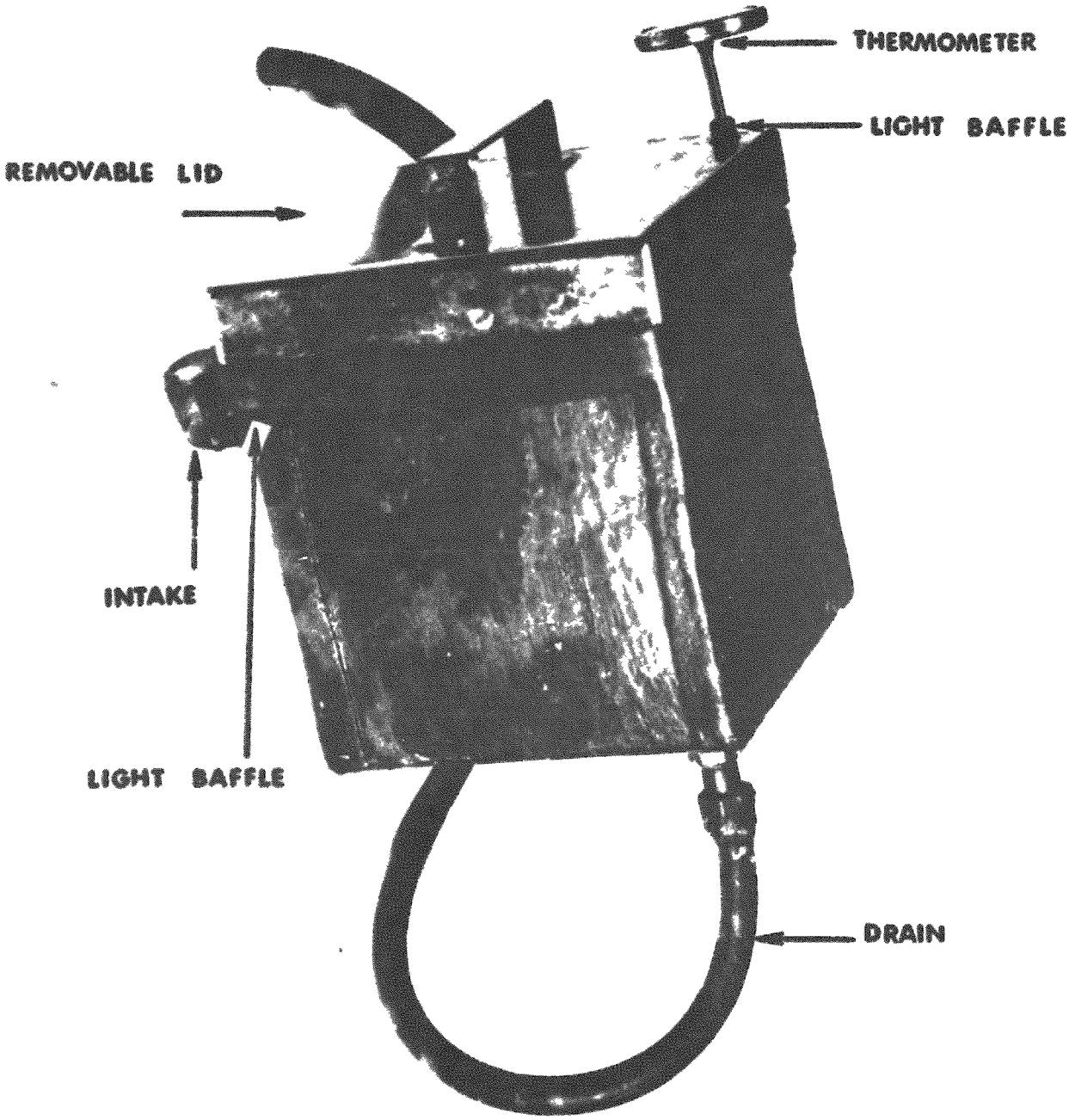

FIG. 2 NUCLEAR EMULSION DEVELOPING TANK

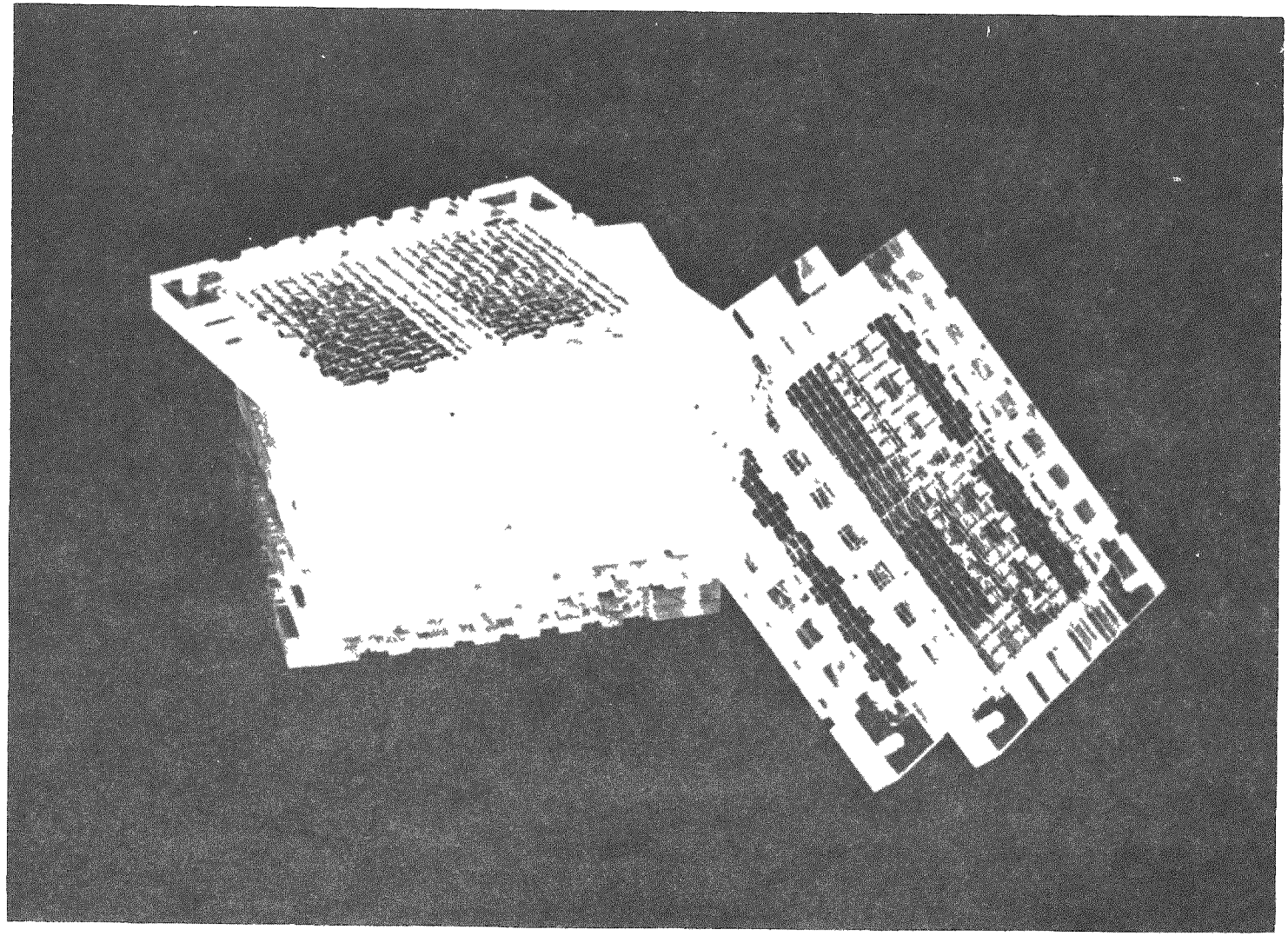

FIG. 3 NUCLEAR EMULSION DEVELOPING RACKS

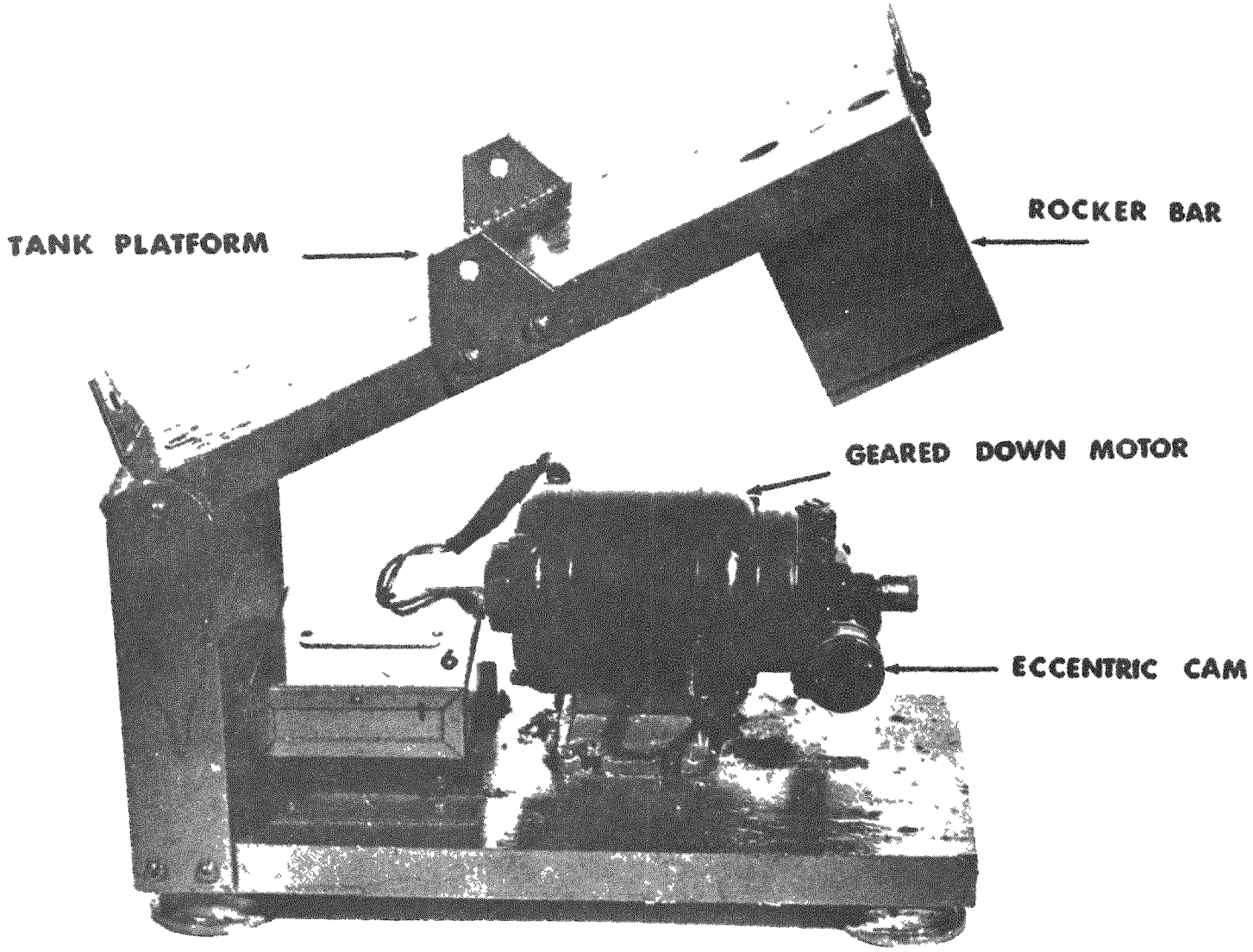

FIG. 4 ROCKER FOR SOLUTION AGITATION

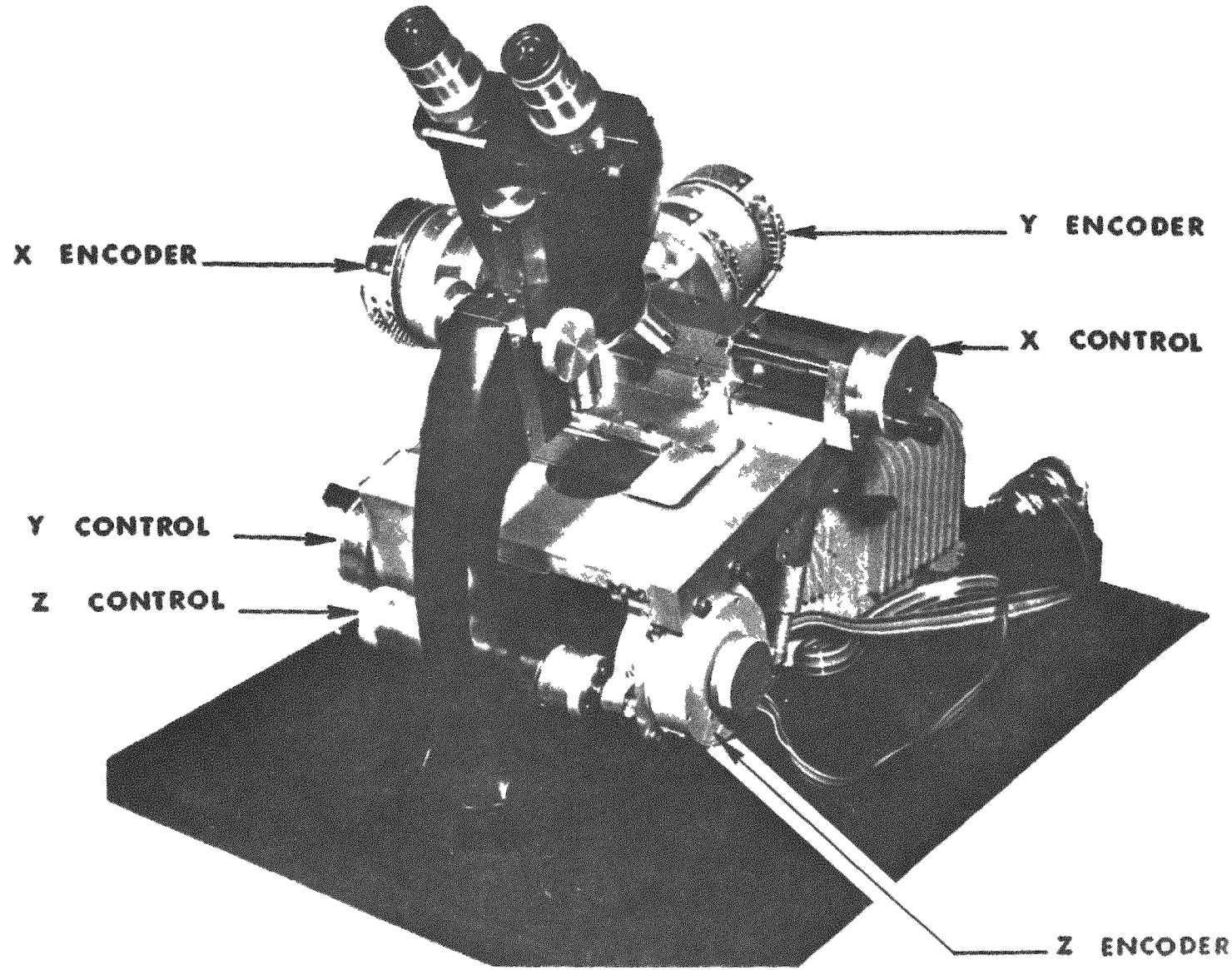

FIG. 5 SCANNING MICROSCOPE FOR NUCLEAR EMULSIONS

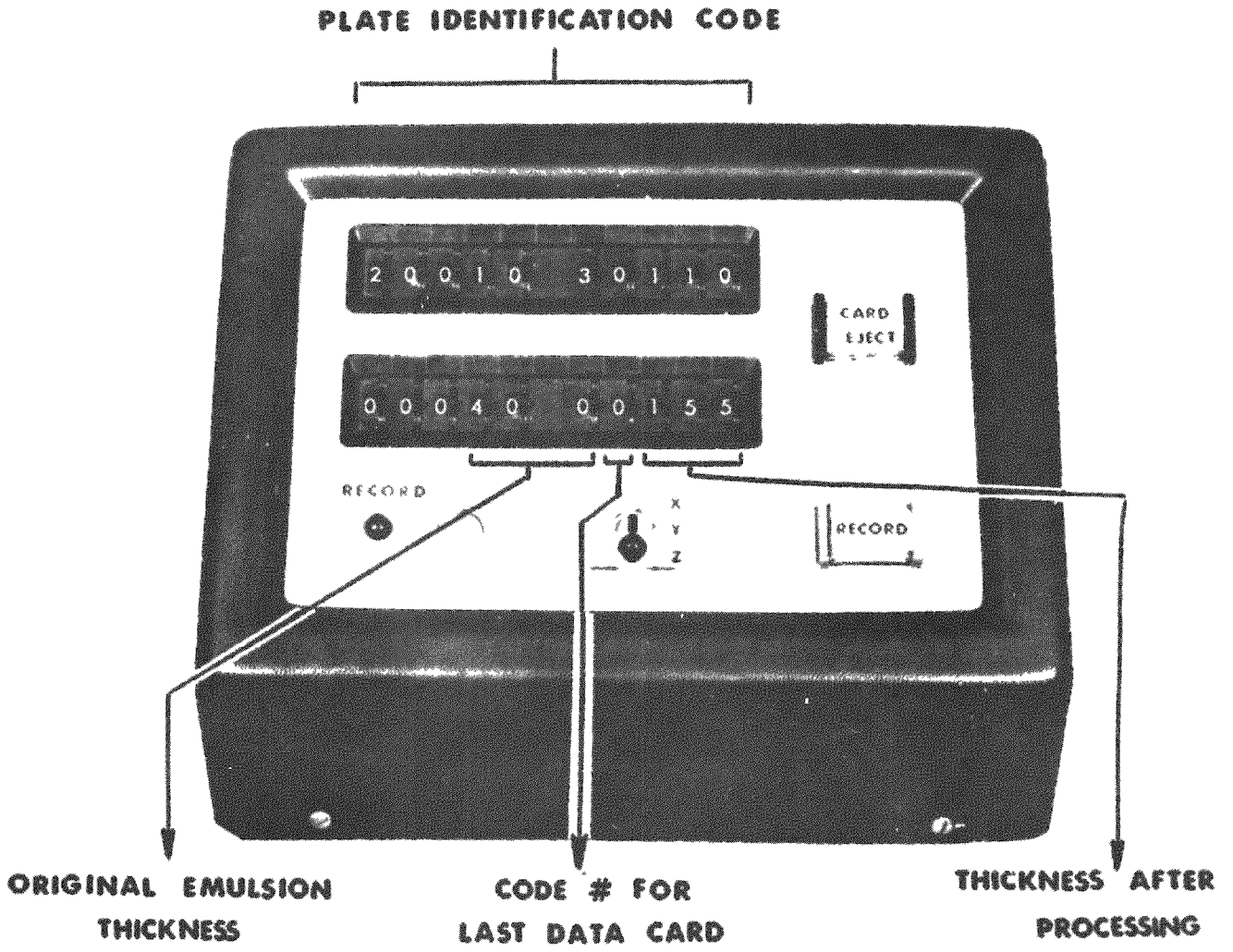

FIG. 6 CONTROL BOX

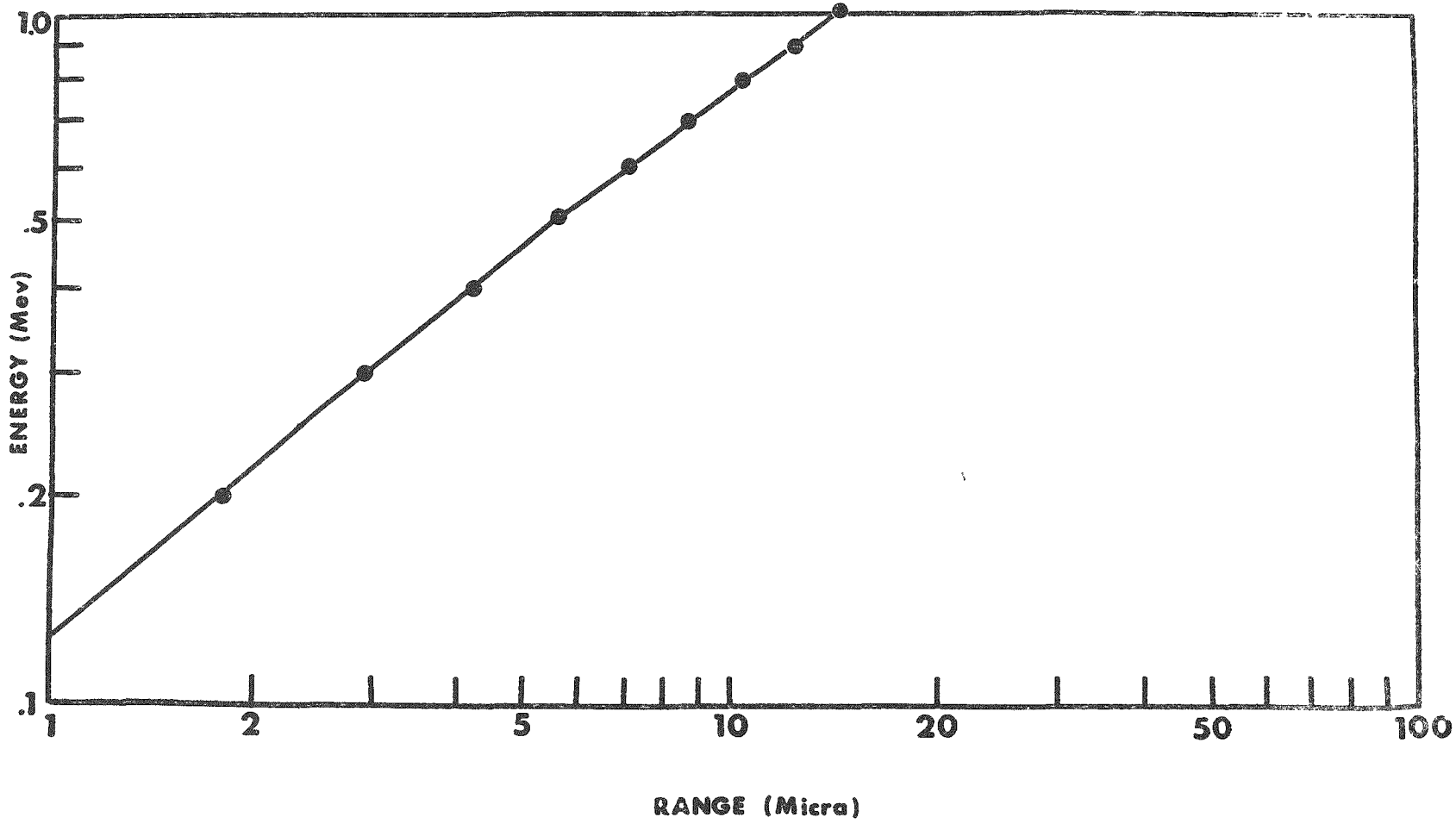

Figure 7. Range-energy curve.

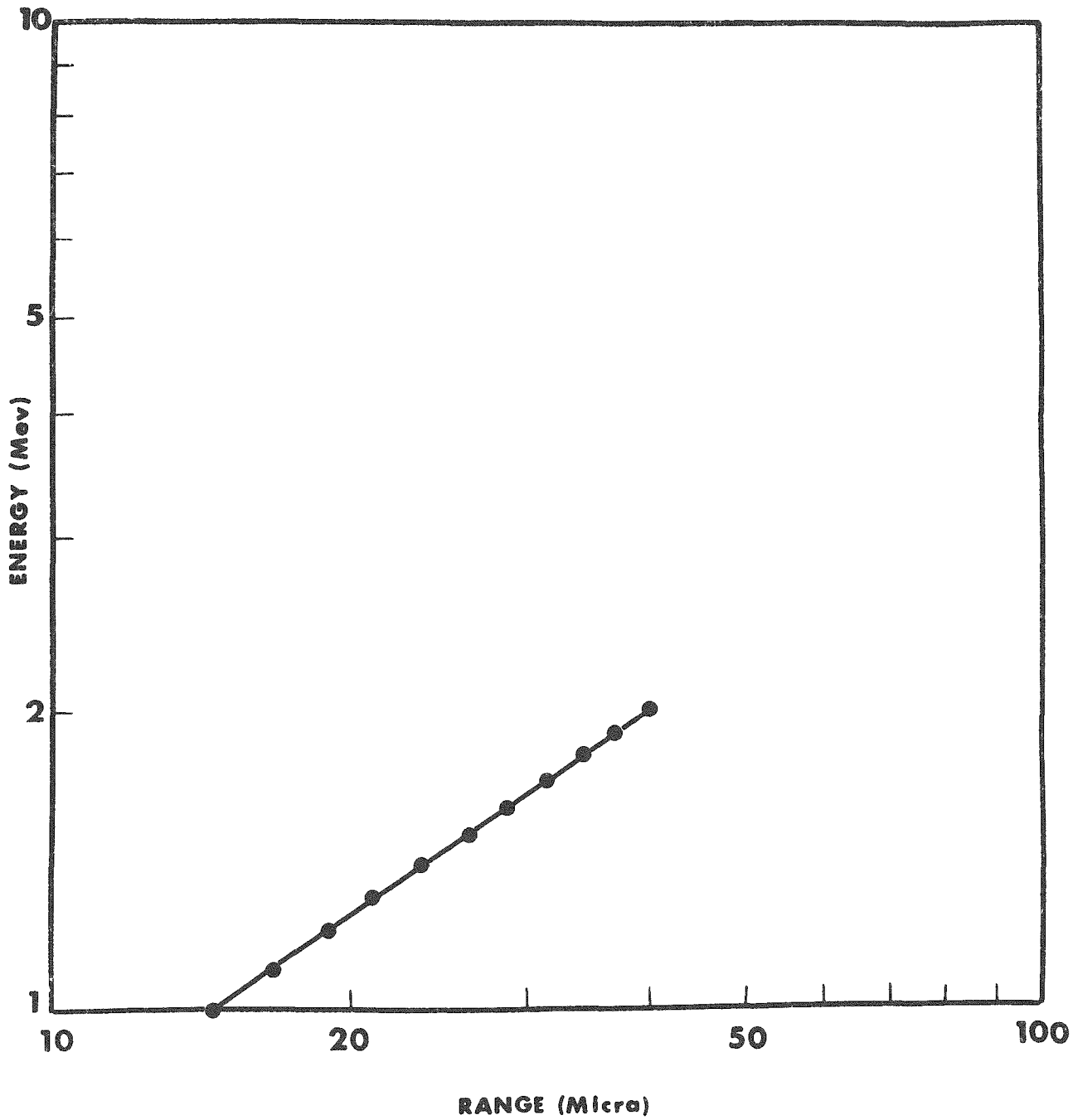

Figure 8. Range-energy curve.

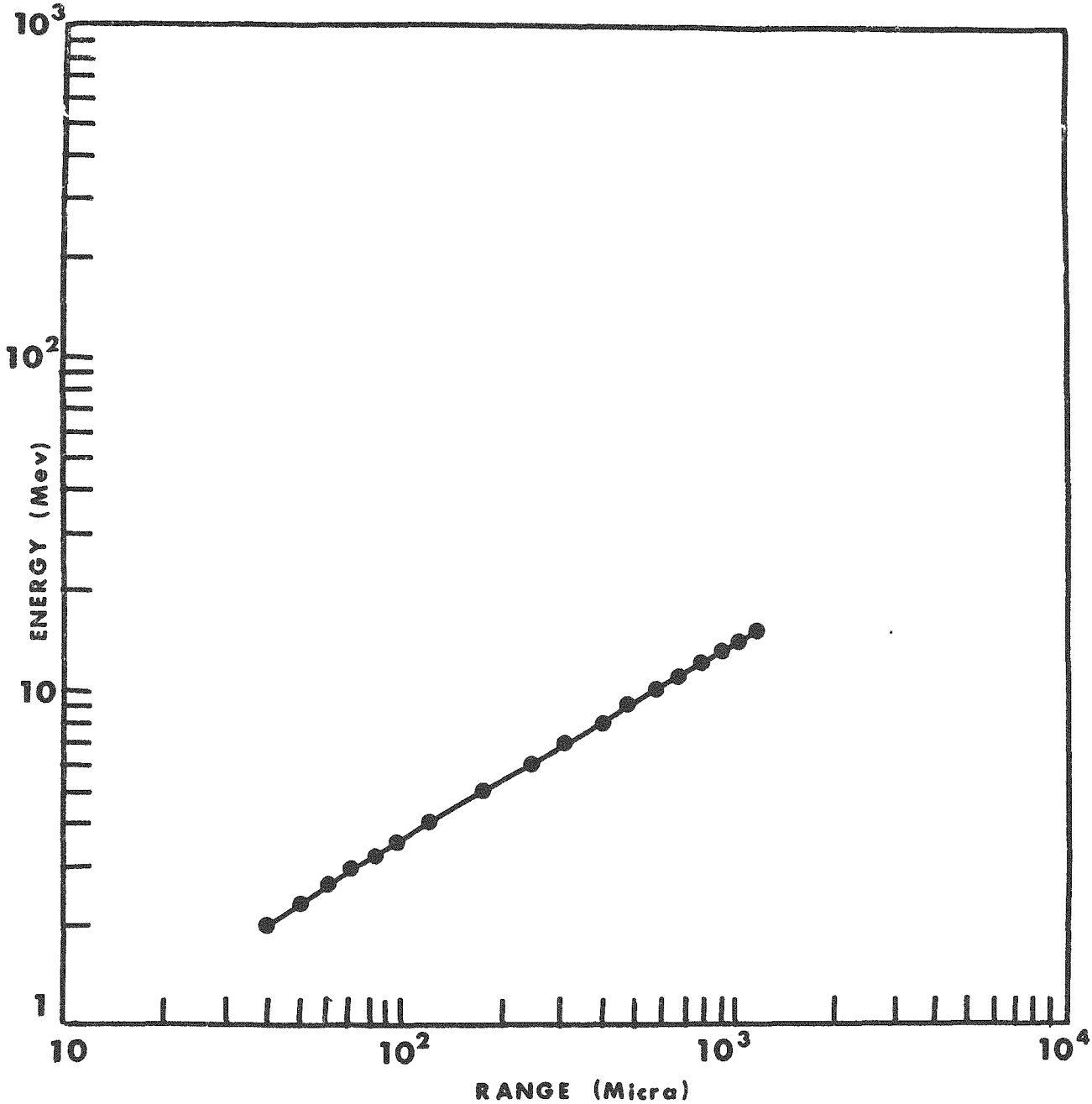

Figure 9. Range-energy curve.

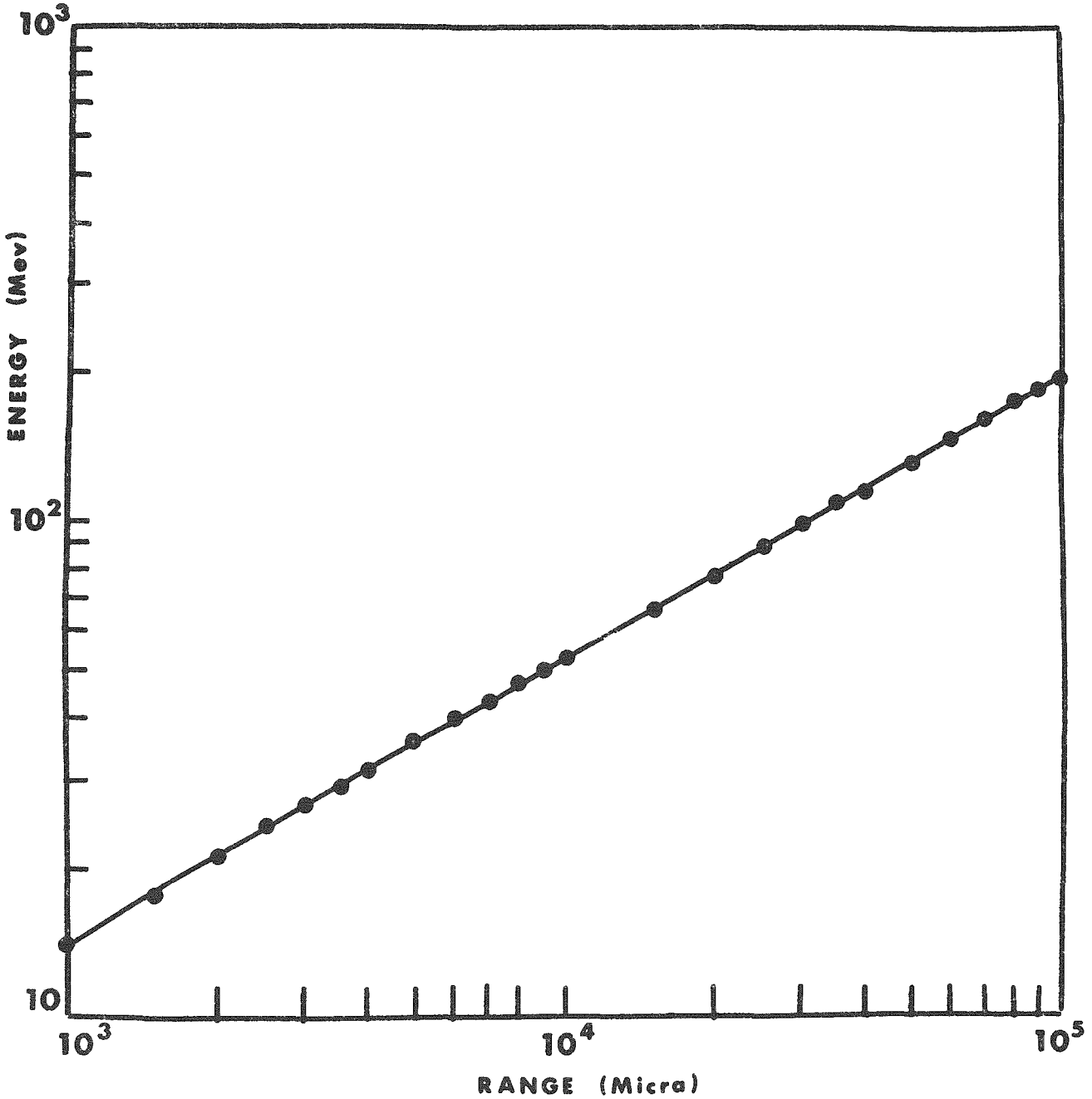

Figure 10. Range-energy curve.

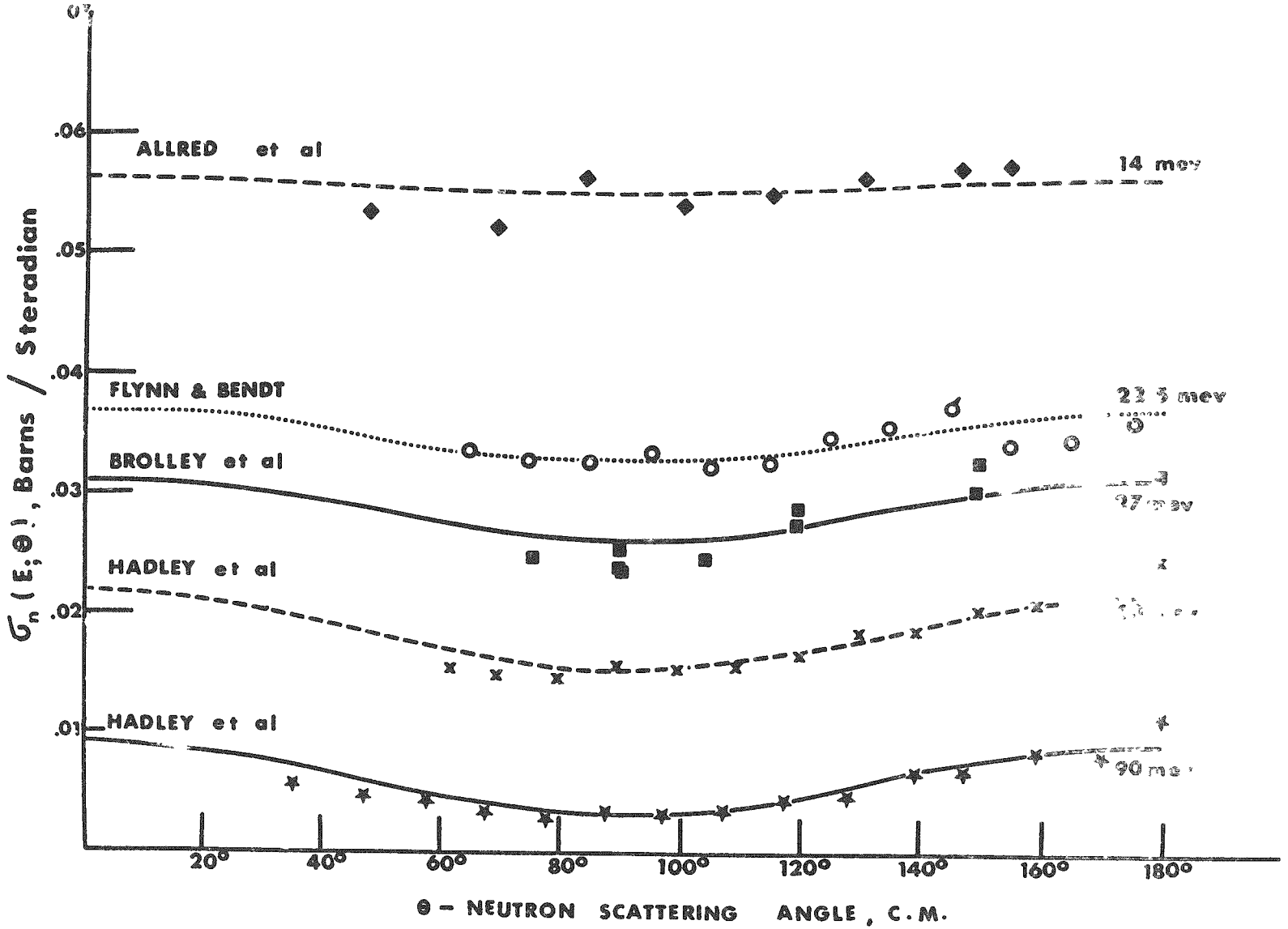

Figure 11. A comparison of Gammel's differential scattering cross section, in the center of mass, with some of the experimental data.

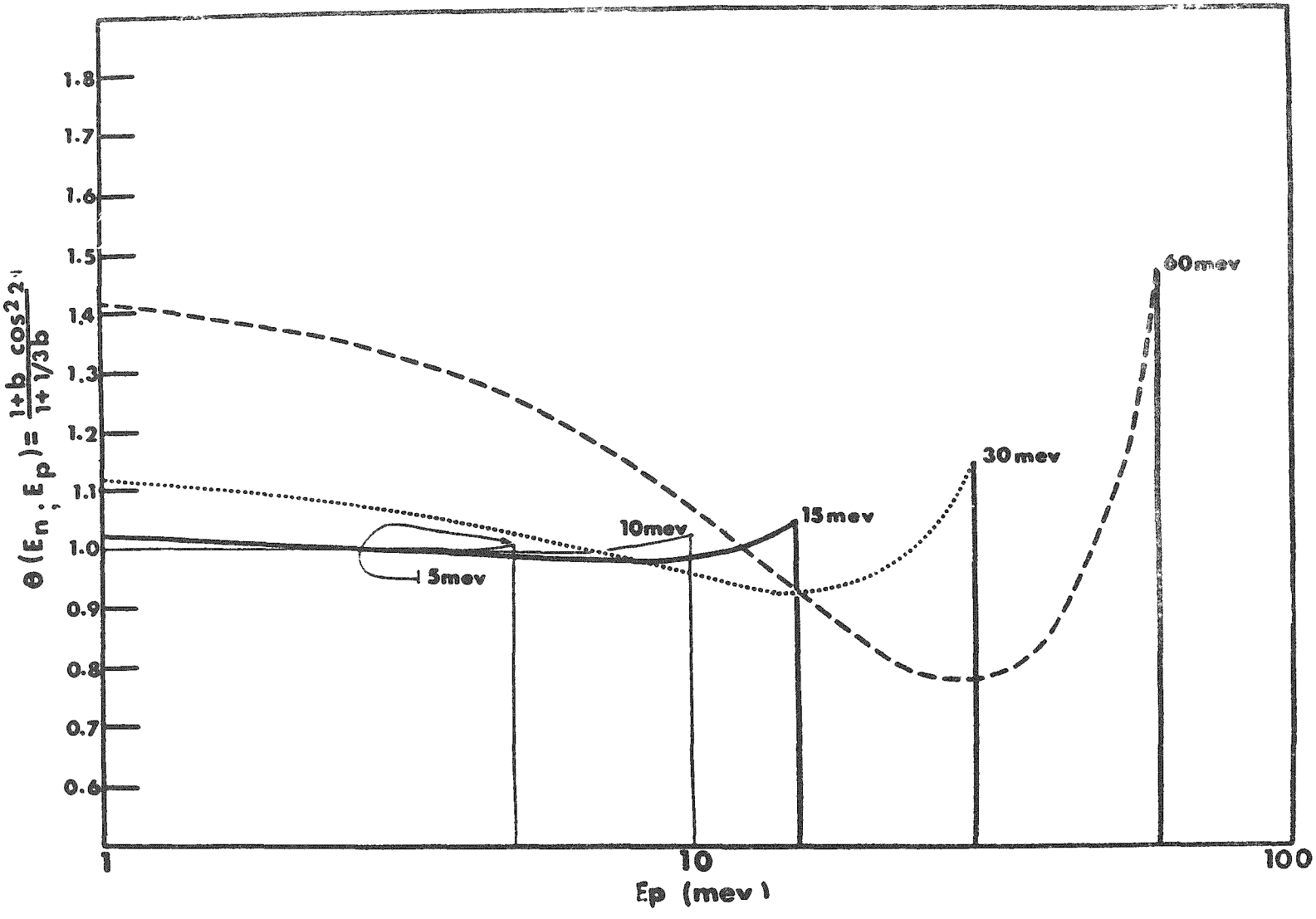

Figure 12. The recoil proton spectrum in laboratory coordinates, per unit proton, for incident monochromatic neutrons from 5 to 60 MeV.

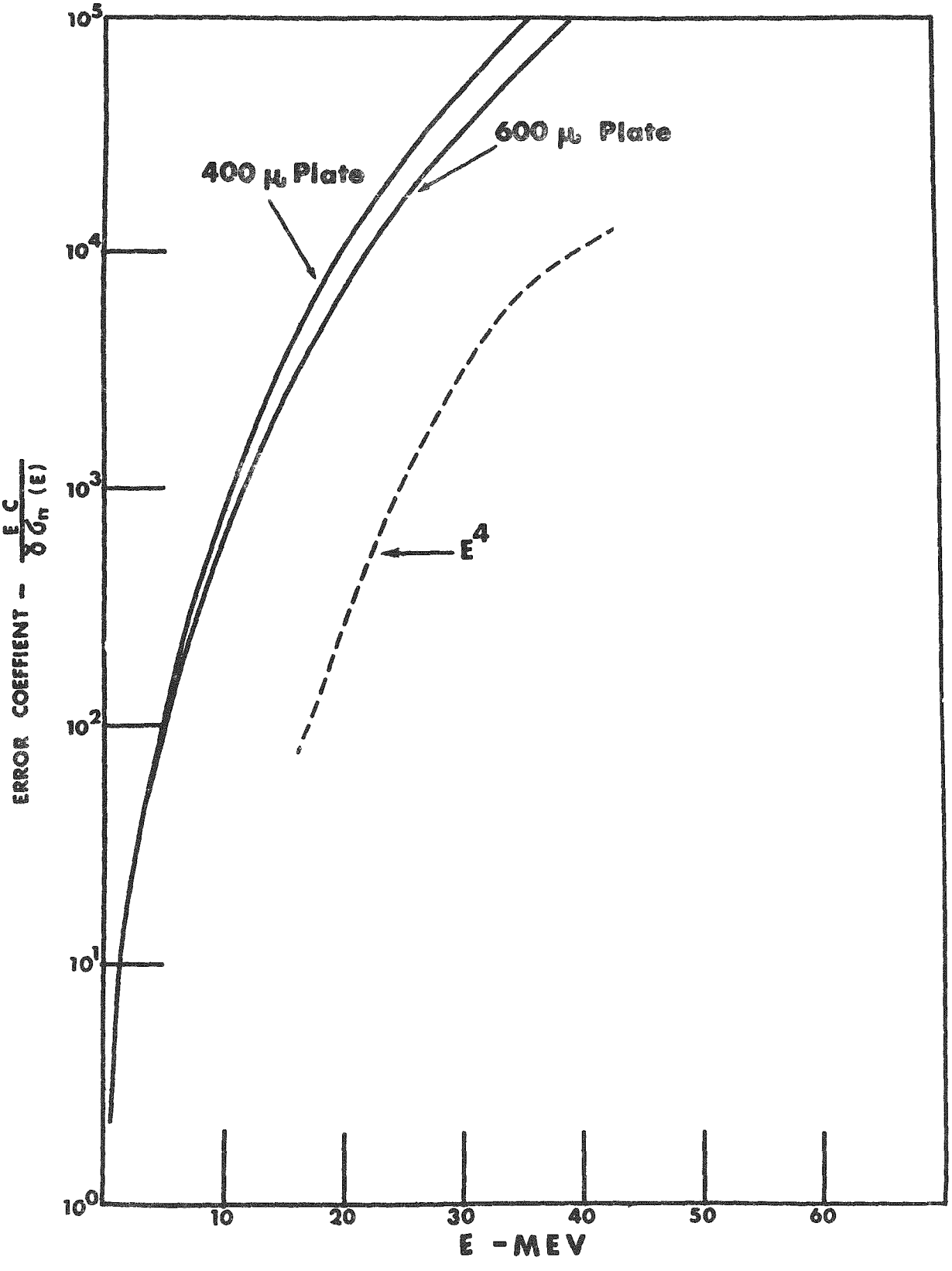

Figure 13. The dependence on neutron energy of the error coefficient, a factor that multiplies the standard deviation, for 2 plate thicknesses.

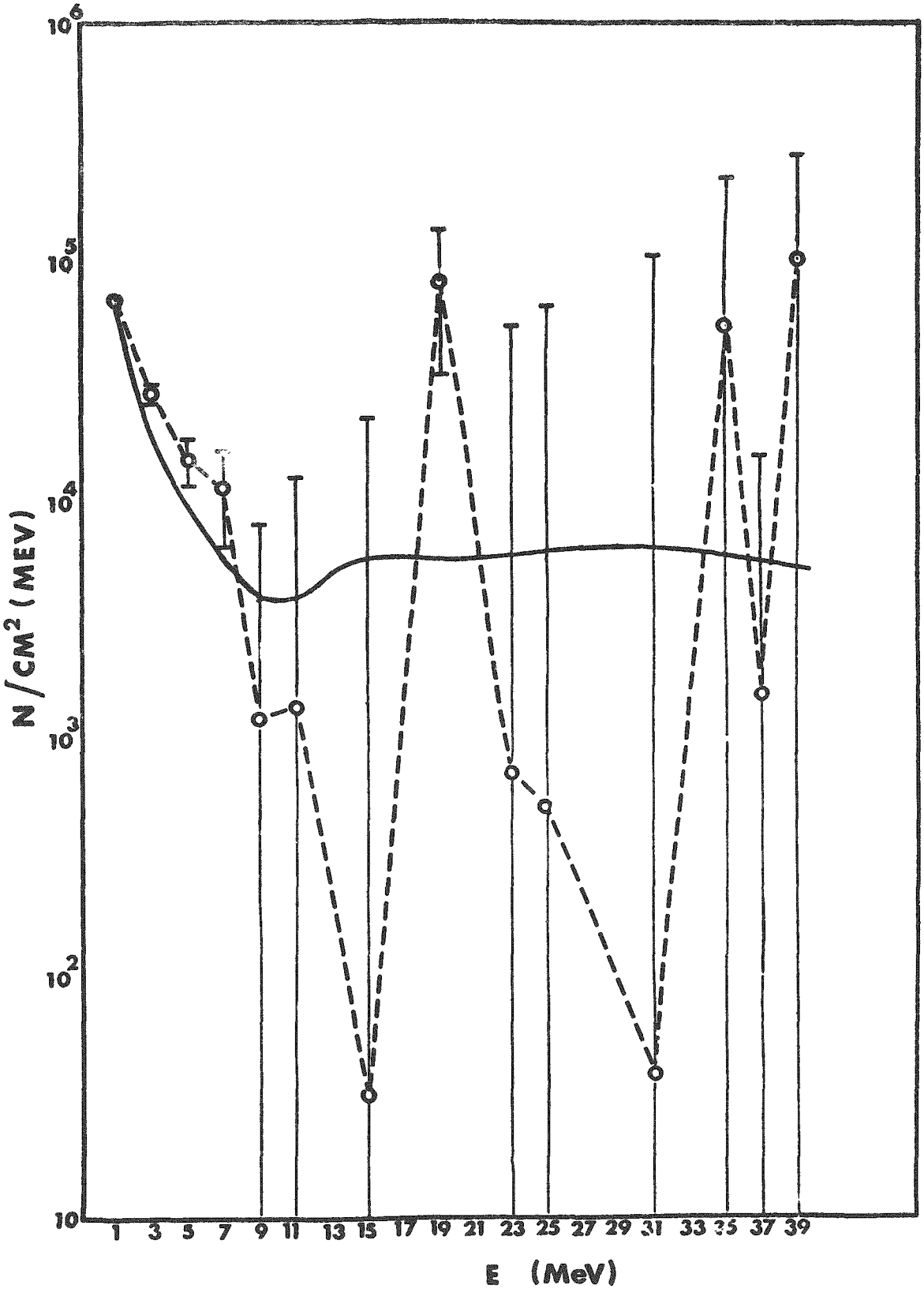

Figure 14. Smoothed and unsmoothed neutron spectra from an Ilford plate exposed to stray cosmotron neutron radiation.

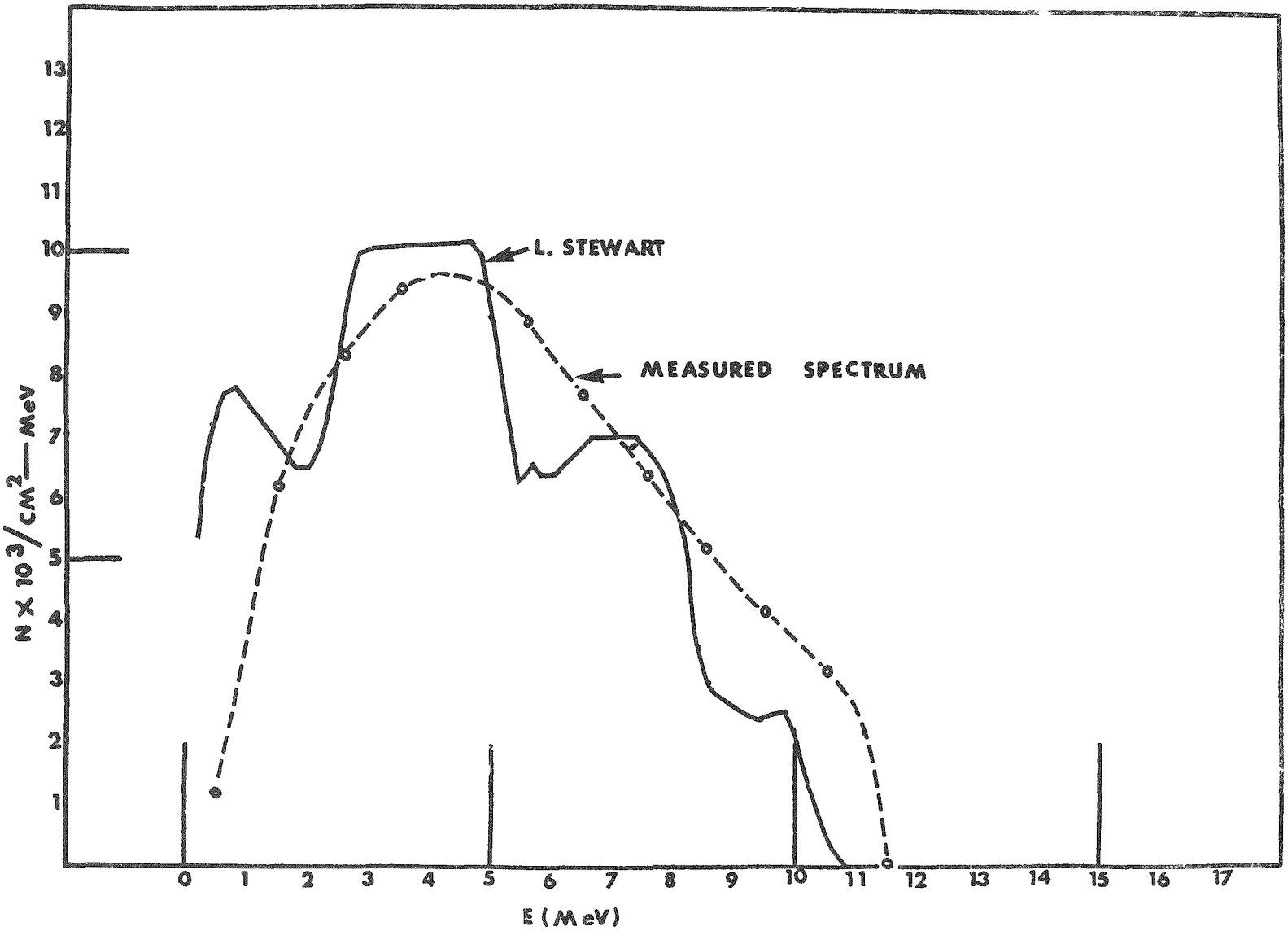

Figure 15. The measured neutron spectrum from a Pu Be neutron source, as compared with Stewart's measurement.

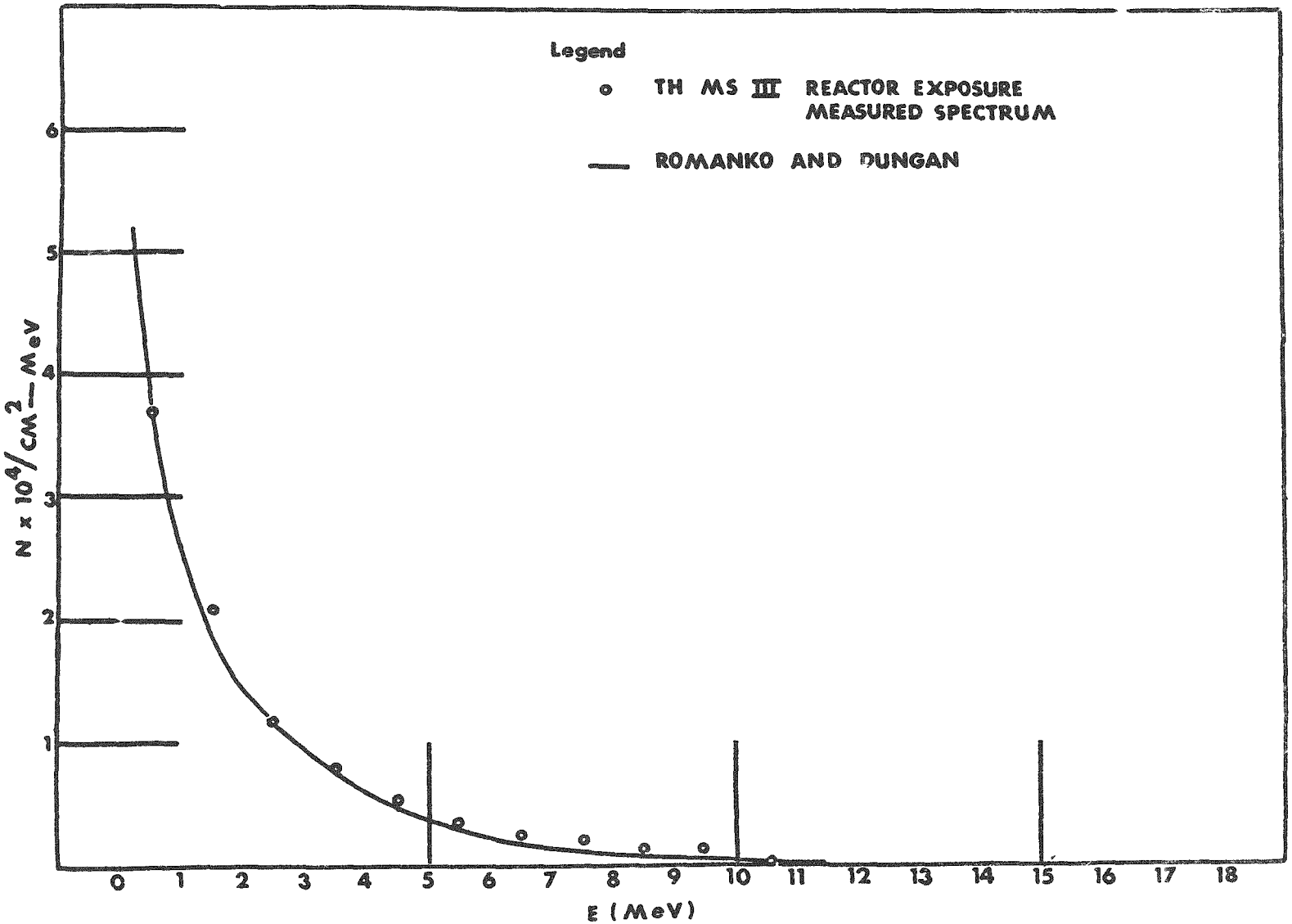

Figure 16. A measured reactor leakage spectrum as compared with the representation of Romanko and Dungan.

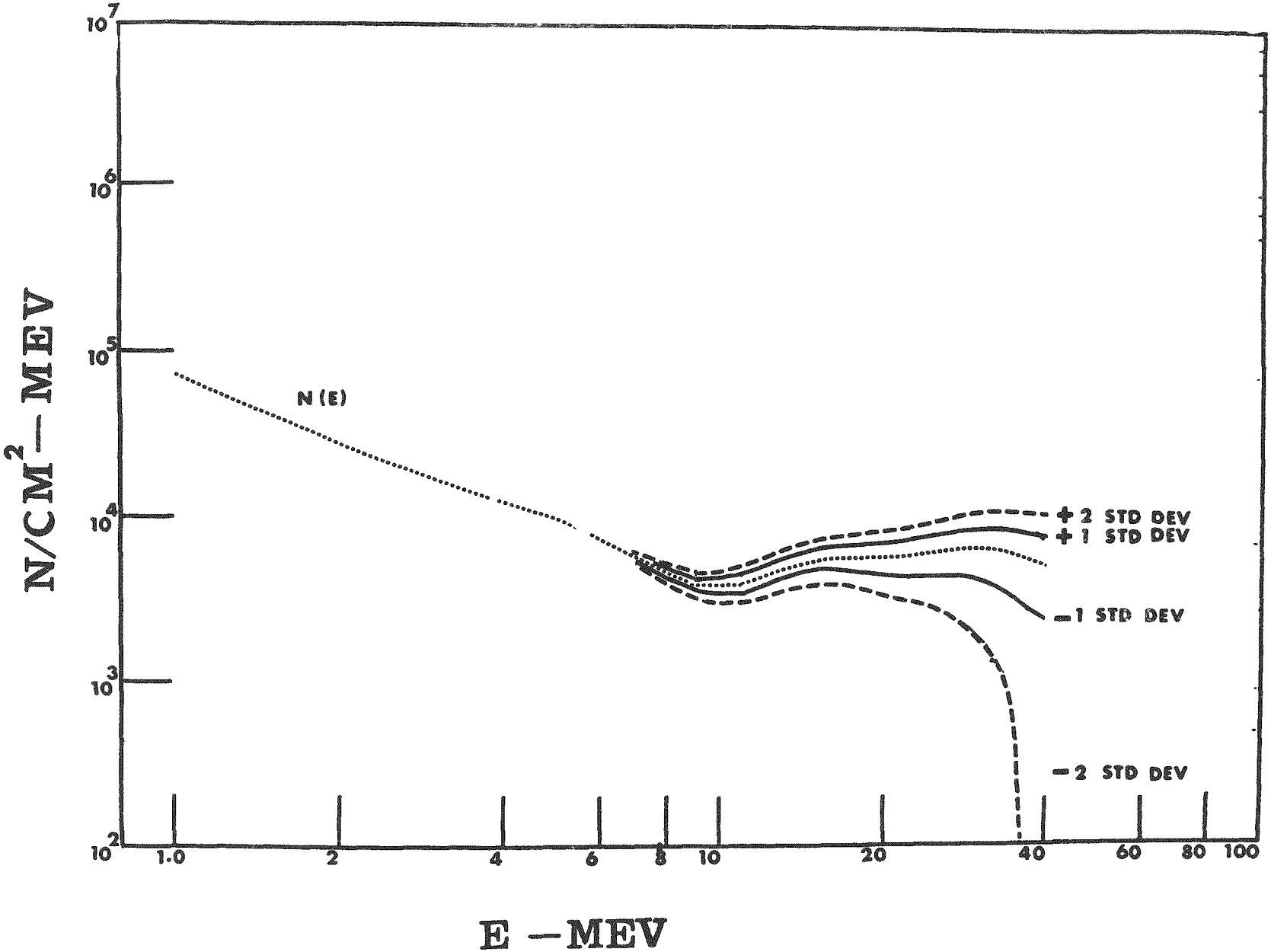

Figure 17. The measured stray neutron spectrum from the south wall of the cosmotron, with associated standard deviations, from equation (56).

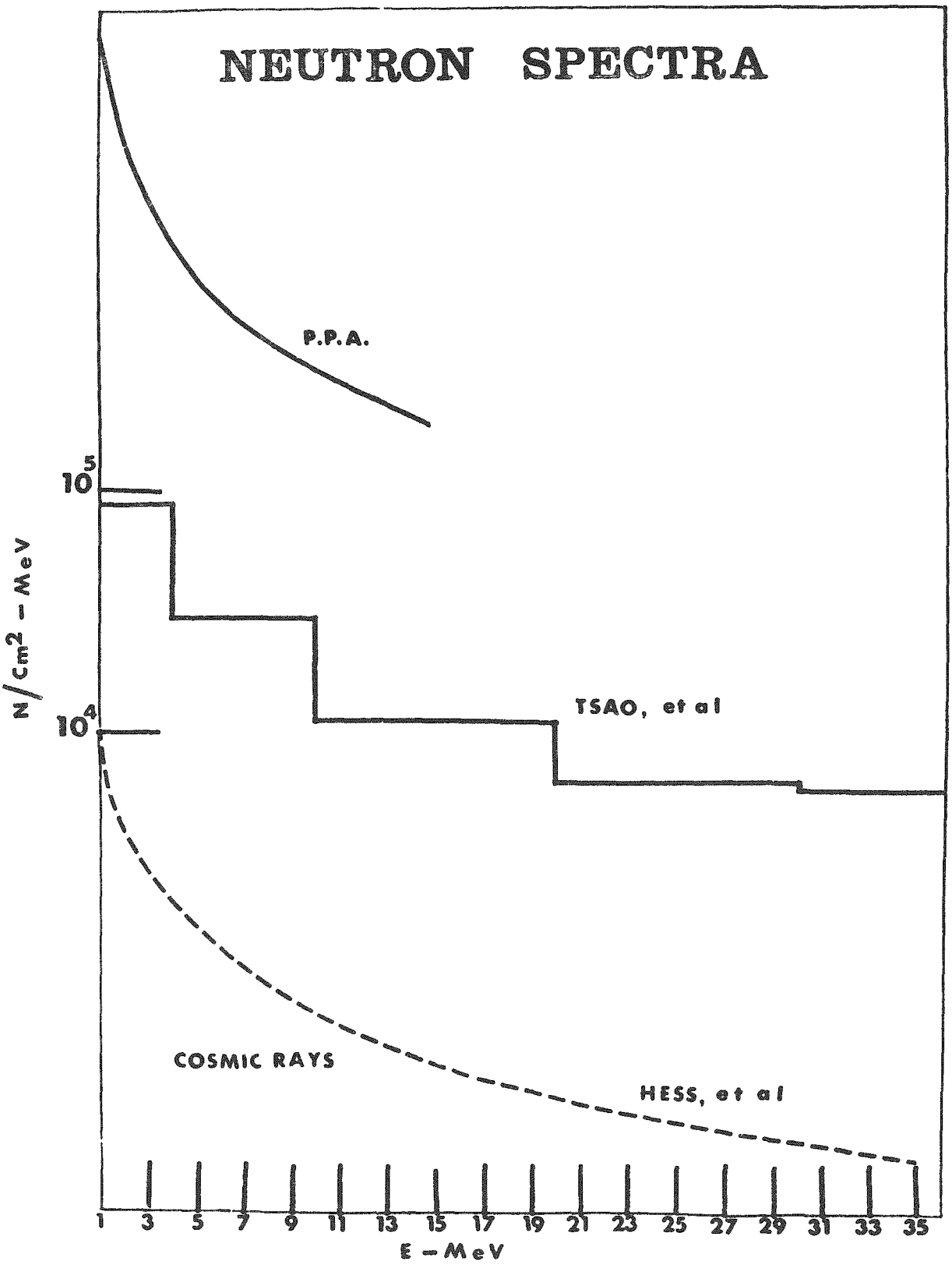

Figure 18. The measured stray neutron spectrum from the Princeton-Pennsylvania Accelerator, as compared with the calculations of Tsao et al, and with the cosmic ray spectrum of Hess et al.

APPENDIX--1 FORTRAN PROGRAMS TO OBTAIN THE RECOIL PROTON SPECTRUM FROM THE RAW DATA

```
*FANDK1410
**    RECOIL PROTON ENERGIES AND CORRECTION FACTORS OBTAINED FROM THE
**    COORDINATES OF THE END POINTS OF THE TRACKS
      DIMENSION E(5),CF(5)
      READ 1,TH
      N=0
   18 I=0
   15 READ 2,ITEST,IT,IX1,IY1,IZ1,IX2,IY2,IZ2
      N=N+1
      I=I+1
      XY=(IX1-IX2)**2+(IY1-IY2)**2
      Z=(IZ1-IZ2)**2
      T=IT
      C=(TH/T)**2
      R=SQRTF(XY+C*Z)
      IF(R-TH)3,4,4
    4 CF(I)=2.*R/TH
      GOTO5
    3 CF(I)=2.*TH/(2.*TH-R)
    5 IF(R-14.5)6,7,7
    7 IF(R-39.7)8,9,9
    9 IF(R-1114.6)10,10,11
   11 E(I)=0.251*(R**0.581)
      GOTO12
   10 E(I)=0.013089*(SQRTF(1557.52*R+47761.7)-176.5)
      GOTO12
    8 E(I)=0.0925926*(SQRTF(21.6*R+109.69)-9.5)
      GOTO 12
    6 E(I)=0.0757576*(SQRTF(26.4*R+62.41)-7.9)
   12 IF(ITEST)13,14,13
   14 IF(I-5)15,16,16
   16 PUNCH 17,(E(J),CF(J),J=1,5)
```

```
      GOTO 18
   13 PUNCH 17,(E(J),CF(J),J=1,I)
      PRINT 19,N
      CALL EXIT
    1 FORMAT(F5.0)
    2 FORMAT(16X,I1,I3,1X,I5,1X,I5,1X,I3,2X,I5,1X,I5,1X,I3)
   17 FORMAT( 5(F8.3,F8.3))
   19 FORMAT(1H ,35H THE TOTAL NO. OF TRACKS SCANNED IS,I7)
       END
```

```
*LDISKPROSP
*FANDK0806
**RECOIL PROTON SPECTRUM FROM PROTON ENERGIES AND CORRECTION FACTORS

      DIMENSION E(200),C(200),P(200),IP(200)
      DO 5 I=1,200
      P(I)=0.
    5 IP(I)=0
      READ600
      READ 1,DE,AK
      K=AK
      M=K
      L=200
    6 READ 2,(E(I),C(I),I=1,L)
      DO 3 I=1,L
      J=(E(I)+DE)/DE
      IF(J-200)202,202,203
  202 IP(J)=IP(J)+1
      P(J)=P(J)+C(I)
      GOTO3
  203 TYPE 107,E(I)
    3 CONTINUE
      M=M-L
      IF(M)9,9,10
   10 IF(L-M)6,8,8
    8 L=M
      GOTO 6
    9 I=200
   13 IF(IP(I))11,12,11
   12 I=I-1
      GOTO 13
   11 NA=I
      E(1)=DE/2.
      DO 14 I=2,NA
   14 E(I)=E(I-1)+DE
      PUNCH 101,(E(I),P(I),IP(I),I=1,NA)
      PRINT 600
      PRINT 601
      PRINT702, (E(I),P(I),IP(I),I=1,NA)
```

```
      CALL EXIT
    1 FORMAT(F5.2,F7.0 )
    2 FORMAT(5(F8.3,F8.3))
  107 FORMAT(5X,2HE=,F12.3)
  101 FORMAT(5X,F7.2,5X,F12.3,5X,F12.3)
  702 FORMAT(1H ,5X,3HE= ,F7.2,5X,6HP(E)= ,F12.3,5X,7HP(UE)= ,F12.3)
  601 FORMAT(//)
  600 FORMAT(1H0,51H
      END
```

```
**     NEUTRON SPECTROMETRY BY MEANS OF THE GOLD-SCOFIELD METHOD AND

**     ZERO ORDER DATA SMOOTHING.

*LDISKSNYDER
      FUNCTION SNYDER(E,I)
      DIMENSION E(200)
      IF(E(I)-1.E-04)1,1,2
1     SNYDER=(.031+296.*E(I))*1.E-08
      RETURN
2     IF(E(I)-.0381)3,3,4
3     SNYDER=.0606*1.E-08
      RETURN
4     IF(E(I)-2.752)5,5,6
5     SNYDER=0.31*(E(I)**.5)*1.E-08
      RETURN
6     SNYDER=0.42*(E(I)**.2)*1.E-08
      RETURN
      END
```

```
*LDISK
      FUNCTION DIFF (E,I,J)
      DIMENSION E(200)
      B=2.*(E(I)/90.)**2
      COSINE=2.*E(J)/E(I)-1.
      DIFF=(1.+B*COSINE**2)/(1.+B/3.)
      RETURN
      END
```

```
*LDISK
      FUNCTION HCROSS (E,N)
      DIMENSION E(200)
      PI=3.1415926536
      A=1.206
      B=-1.86
      C=.09415
      D=1.306E-04
      F=.4223
      G=.13
      HCROSS=3.*PI/(A*E(N)+(B+C*E(N)+D*E(N)*E(N))**2)+PI/.A*E(N)+(F+G*E
     1(N))**2)
      RETURN
      END
```

```
*LDISKCORR
      FUNCTION CORR(E,LOOP,T)
      DIMENSION E(200)
      IF(E(LOOP)-1.6)900,901,902
  902 IF(E(LOOP)-4.9)901,901,903
  900 RANG=13.8*E(LOOP)**1.5+0.6
      GOTO 904
  901 RANG=5.1*E(LOOP)**2+9.7*E(LOOP)+0.2
      GOTO 904
  903 RANG=(3.984*E(LOOP))**1.721
  904 IF(T-RANG)905,906,906
  905 CORR=(2.*RANG)/T
      RETURN
  906 CORR=(2.*T)/(2.*T-RANG)
      RETURN
      END
```

```
*LDISKHERM3
*IF TRACE
*ALL STATEMENT MAP
*ARITHMETIC TRACE
*LIST PRINTER
** HERM3, SMOOTHED NEUTRON SPECTRUM WITH BEST FIT TRUNCATION(EG+G).

      DIMENSION E(200),P(200) ,C(200),D(200),S(200),X(200)
      READ 302,01,02,03,04,05,06,07,08,09,010,011,012,013,014,015,016,
     1017,018
      PUNCH302,01,02,03,04,05,06,07,08,09,010,011,012,013,014,015,016,
     1017,018
      PRINT 100,01,02,03,04,05,06,07,08,09,010,011,012,013,014,015,016,
     1017,018
      PRINT 105
      READ 1,K,T
      PUNCH 999,K
      SUM=0.
      DO 2 I=1,K
      READ 3,E(I),P(I)
      IF(SENSE SWITCH 34)102,103
102   PRINT 104
      PRINT 100,01,02,03,04,05,06,07,08,09,010,011,012,013,014,015,016,
     1017,018
103   PRINT 9, E(I),P(I)
      SUM=SUM+P(I)
      C(I)=P(I)
2     D(I)=E(I)/(.03645*HCROSS(E,I))
      PRINT 314, SUM
      DELT=E(2)-E(1)
      DO 25 I=1,100
      RS=0.
      DO 4 J=1,K
      AX=0.
      DO 5 M=J,K
      X(M)=C(M)*DIFF(E,M,J)+AX
5     AX=X(M)
      S(J)=C(J)*P(J)/AX
    4 C(J)=S(J)
```

```
      DO 20 M=1,K
      RESQ=(X(M)-P(M))**2+RS
20    RS=RESQ
      IF(I-1)25,25,22
22    IF(RESQ-REST)25,90,90
25    REST=RESQ
90    DO 6 I=1,K
6     S(I)=S(I)/DELT*D(I)
      PRINT 105
      HART=0.
      PART=0.
      DO 16 J=1,K
      SSS=E(J)/SQRTF(2.*3.14159)
      SUM=0.
      DO 15 I=1,K
      IF(S(I))101,15,101
101   IF(E(J)-E(I))50,62,50
50    PALLAS=(E(J)-E(I))/SSS
      PALLAS=ABSF(PALLAS)
      IF(PALLAS-10.)70,70,15
70    SUM=SUM+S(I)*.5642/SSS*EXP(-(E(J)-E(I))**2/(2.*SSS*SSS))/SQRTF(8.)
      GO TO 15
62    SUM=SUM+.5642/SSS*S(I)/SQRTF(8.)
15    CONTINUE
      CN=DELT*SUM
      STD=SQRTF(CN*CORR(E,J,T)/(DELT*.03645*HCROSS(E,J)))*SQRTF(SQRTF(2.
     1))/SQRTF(8.)
      IF(SENSE SWITCH 34) 106,107
106   PRINT 104
      PRINT 100,01,02,03,04,05,06,07,08,09,010,011,012,013,014,015,016,
     1017,018
      PRINT 105
107   PRINT 7,E(J),CN,STD
      PUNCH400,E(J),CN
      PART=CN*SNYDER(E,J)+PART
      HART=HART+CN
16    CONTINUE
      PART=PART/HART
```

```
      HART=HART*DELT
      PRINT 301, PART,HART
      CALL EXIT
1     FORMAT(I5,F4.0)
    3 FORMAT(5X,F7.2,5X,F12.3)
105   FORMAT(1H0)
302   FORMAT(18A4)
104   FORMAT(1H1)
7     FORMAT(1H ,5X,2HE=,F7.2,5X,6HN(E)= ,F12.3,5X,9HSTD DEV= F12.3)
  400 FORMAT(5X,2HE=,F7.2,5X,6HN(E)= ,F12.3)
314   FORMAT(1H0,14HPROTONS/CM-3= F12.3)
9     FORMAT(1H ,5X,2HE=,F7.2,5X,6HP(E)= ,F12.3)
100   FORMAT(1H0,18A4)
301   FORMAT(1H0,E10.3,2X,11HRADS/N/CM-2/1H F12.3,2X,6HN/CM-2/1H1)
999   FORMAT(I4)
      END
```

```
*IF TRACE
*ALL STATEMENT MAP
*ARITHMETIC TRACE
*LIST PRINTER
*LDISKRUG2
**RUG2, UNSMOOTHED NEUTRON SPECTRUM USING A BEST FIT CRITERION(EG+G).

      DIMENSION E(200),P(200) ,C(200),D(200),S(200),X(200)
      READ 302,01,02,03,04,05,06,07,08,09,010,011,012,013,014,015,016,
     1017,018
      PUNCH302,01,02,03,04,05,06,07,08,09,010,011,012,013,014,015,016,
     1017,018
      PRINT 100,01,02,03,04,05,06,07,08,09,010,011,012,013,014,015,016,
     1017,018
      PRINT 105
      READ 1,K,T
      PUNCH 999,K
      SUM=0.
      DO 2 I=1,K
      READ 3,E(I),P(I)
      IF(SENSE SWITCH 34)102,103
102   PRINT 104
      PRINT 100,01,02,03,04,05,06,07,08,09,010,011,012,013,014,015,016,
     1017,018
103   PRINT 9, E(I),P(I)
      SUM=SUM+P(I)
      C(I)=P(I)
2     D(I)=E(I)/(.03645*HCROSS(E,I))
      PRINT 314, SUM
      DELT=E(2)-E(1)
      DO 25 I=1,100
      RS=0.
      DO 4 J=1,K
      AX=0.
      DO 5 M=J,K
      X(M)=C(M)*DIFF(E,M,J)+AX
5     AX=X(M)
      S(J)=C(J)*P(J)/AX
```

```
    4 C(J)=S(J)
      DO 20 M=1,K
      RESQ=(X(M)-P(M))**2+RS
20    RS=RESQ
      IF(I-1)25,25,22
22    IF(RESQ-REST)25,90,90
25    REST=RESQ
90    DO 6 I=1,K
6     S(I)=S(I)/DELT*D(I)
      PRINT 105
      HART=0.
      PART=0.
      DO 16 J=1,K
      CN=S(J)
      STD=SQRTF(P(J)/CORR(E,J,T)*2.)*E(J)*CORR(E,J,T)/(DELT*.03645*HCROS
     1S(E,J))
      IF(SENSE SWITCH 34) 106,107
106   PRINT 104
      PRINT 100,01,02,03,04,05,06,07,08,09,010,011,012,013,014,015,016,
     1017,018
      PRINT 105
107   PRINT 7,E(J),CN,STD
      PUNCH 998, E(J),CN
      PART=CN*SNYDER(E,J)+PART
      HART=HART+CN
16    CONTINUE
      PART=PART/HART
      HART=HART*DELT
      PRINT 301, PART,HART
      CALL EXIT
999   FORMAT(I4)
1     FORMAT(I5,F4.0)
    3 FORMAT(5X,F7.2,5X,F12.3)
105   FORMAT(1H0)
302   FORMAT(18A4)
104   FORMAT(1H1)
7     FORMAT(1H ,5X,2HE=,F7.2,5X,6HN(E)= ,F12.3,5X,9HSTD DEV= F12.3)
998   FORMAT(5X,2HE=,F7.2,5X,6HN(E)= ,F12.3)
314   FORMAT(1H0,14HPROTONS/CM-3= F12.3)
```

```
9       FORMAT(1H ,5X,2HE=,F7.2,5X,6HP(E)= ,F12.3)
100     FORMAT(1HO,18A4)
301     FORMAT(1HO,E10.3,2X,11HRADS/N/CM-2/1H F12.3,2X,6HN/CM-2/1H1)
        END
```